Modeling Internal Combustion Engine Three-Piece Oil Control Ring Coupling Reduced Order Oil Transport based on Neural Network

by

Wang Zhang

B.Eng., Automotive Engineering,
Tsinghua Uuniversity, 2017
Submitted to the Department of Mechanical Engineering and
Department of Electrical Engineering and Computer Science
in partial fulfillment of the requirements for the degree of

Master of Science in Mechanical Engineering and
Master of Science in Electrical Engineering and Computer Science

at the

MASSACHUSETTS INSTITUTE OF TECHNOLOGY

May 2020

Author . . . .
Department of Mechanical Engineering and
Department of Electrical Engineering and Computer Science
May 15, 2020

Certified by . . . .
Tian Tian
Principal Research Engineer, Department of Mechanical Engineering
Thesis Supervisor

Certified by . . . .
Luca Daniel
Professor, Department of Electrical Engineering and Computer Science
Thesis Reader

Accepted by . . . .
Nicolas Hadjiconstantinou
Professor of Mechanical Engineering
Chair, Department Committee on Graduate Students

Accepted by . . . .
Leslie A. Kolodziejski
Professor of Electrical Engineering and Computer Science
Chair, Department Committee on Graduate Students

Modeling Internal Combustion Engine Three-Piece Oil Control Ring Coupling Reduced Order Oil Transport based on Neural Network

by

Wang Zhang

Submitted to the Department of Mechanical Engineering and
Department of Electrical Engineering and Computer Science
on May 15, 2020, in partial fulfillment of the
requirements for the degree of
Master of Science in Mechanical Engineering and
Master of Science in Electrical Engineering and Computer Science

Abstract

Reducing emission and improving efficiency of internal combustion engines are the major focuses in modern automotive industry. Lubrication oil leakage contributes to particle formation and piston ring friction occupies 1/3 to 1/2 of total mechanical losses in engines. In almost all of modern gasoline engines, three-piece oil control ring (TPOCR) is used considering its low-cost and satisfying oil control performance in low load work conditions. While TPOCR will see high oil consumption at high load, high speed working conditions. This raises our interest in modeling work to predict the TPOCR dynamics and oil transport and explain the oil control mechanism.

This master thesis work is focusing on building a three-piece oil control ring model coupling the oil transport. First, a 2D dynamics model for three pieces is established as the main frame. Second, oil transport in different zones will be modelled in different ways considering the length scales. Specially for the oil movement behind the ring, a novel approach is introduced by using neural networks to learn and run the reduced order modeling of computational fluid dynamics (CFD), to speed up the calculation.

The model is then applied on a 2D laser induced fluorescence (2DLIF) engine and produces consistent simulation results with experimental observation. Further parametric study on oil transport will be discussed to build a complete picture of oil transport around TPOCR.

Thesis Supervisor: Tian Tian
Title: Principal Research Engineer, Department of Mechanical Engineering

Thesis Reader: Luca Daniel
Title: Professor, Department of Electrical Engineering and Computer Science

Acknowledgments

The master degree study in MIT has been one of the most important memories in my lifetime, I feel very lucky to have so many wonderful people helping me going through the last three years and I would like to express my gratitude to them. First and foremost, I would like to thank my advisor, Dr. Tian Tian, who brought me to Sloan Automotive Lab, for his continuous support and inspiration. Exposed to his depth of knowledge and way of thinking, I have achieved professional and personal progress far beyond my expectation. He is more than an academic advisor, but also a life mentor and everyday friend for me. I will always be grateful to him.

I would like my co-advisor and thesis reader Professor Luca Daniel, who brought me to a different view of modelling techniques. I have gained so many ideas and expertise through the intensive discussion with him.

I would like to thank all the members of the Lubrication in Internal Combustion Engines Consortium in the Sloan Automotive Laboratory, who financially supported my graduate study. The consortium members are Mahle, MTU, PSA, Renault, Shell, Toyota, Volkswagen, Volvo Truck, and Weichai Power. Specially, I truly appreciate the collaborations from all the consortium member representatives, your feedbacks have always been the major motivation of my model development.

I would like to thank all my colleagues in the lab, Yang Liu, Tianshi Fang, Zhen Meng, Sebastian Ahling, Chongjie Gu, Qin Zhang, Yuwei Li, Jerome Sacherer, Yulin Pan, Koji Kikuhara, Wei Pu, Xiaofeng Qin, Zhe Chen and our lab administrator Janet Maslow for their support and friendship. It is my fortune to work with you all, my graduate study would not be such smooth without these everyday communications. I would like to thank all the friends I met in the Boston area, for their encouragement and company, bring me joy in the most stressful days.

Finally, I would like the thank my family in China, my aunts' family in local Boston, and my girlfriend always with me, for their immense support, understanding and patience, through the happiness or difficulties in the past years.

Contents

List of Figures

9

Chapter 1

Introduction

1.1 Motivation

Through the automotive history, internal combustion engine has always been the major power sources for vehicles considering its performance, convenience, cost and reliability, despite the challenges from alternatives. In the development of modern internal combustion engines, the research focus falls on fuel economy and pollution emissions, both of them are heavily associated to engine piston ring pack system.

Piston ring pack accounts up to 25% of total mechanical loss in piston power system[1][2], reducing the friction could improve vehicle fuel economy. On the other hand, piston rings are critical components in regulating oil behavior. Undesired engine lubricant leakage into upper part of the piston can potentially lead to pollution and abnormal engine behavior such as shocking[3]. Traditional ways to reduce oil consumption, increasing ring tension for instance, will compromise engine efficiency, and the marginal benefit is limited after ring tension reaches certain threshold. Given the fact that automotive equipped with internal combustion engine will experience varying driving situations, it requires the ring pack system to satisfy different working conditions, from low load to high load, from low speed to high speed, from cold start to maximum power output. All these factors trigger a strong incentive to investigate the system for understanding the mechanisms and inspiring optimization guidelines.

Prior to this work, Tian[4] developed a ring pack system model and a three-piece

oil control ring (TPOCR) model[5] based on axisymmetric assumptions. The ring dynamics and gas flows were explained with these models . Fang[6] describes the oil movement in non-contact regions in the piston ring pack with computational fluid dynamics (CFD) and investigated the lubricant transport patterns in non-contact regions. Inspired by these works, a complete simulation package coupling the oil control ring dynamics and oil transport is established in this thesis to describe a comprehensive picture of oil regulation mechanisms, with efficiency, robustness and practical values to users from automotive industry.

1.2 Piston ring pack system

Fig 1-1 shows the piston, ring pack system and their cross-section schematic in a typical internal combustion engine. When the fuel burns in the combustion chamber, the piston is used to transfer the gas pressure into mechanical work driving the power train. On the piston, there are three grooves to accommodate three rings. The part below the piston ring pack is called piston skirt that contacts with liner (cylinder wall) to balance lateral force.
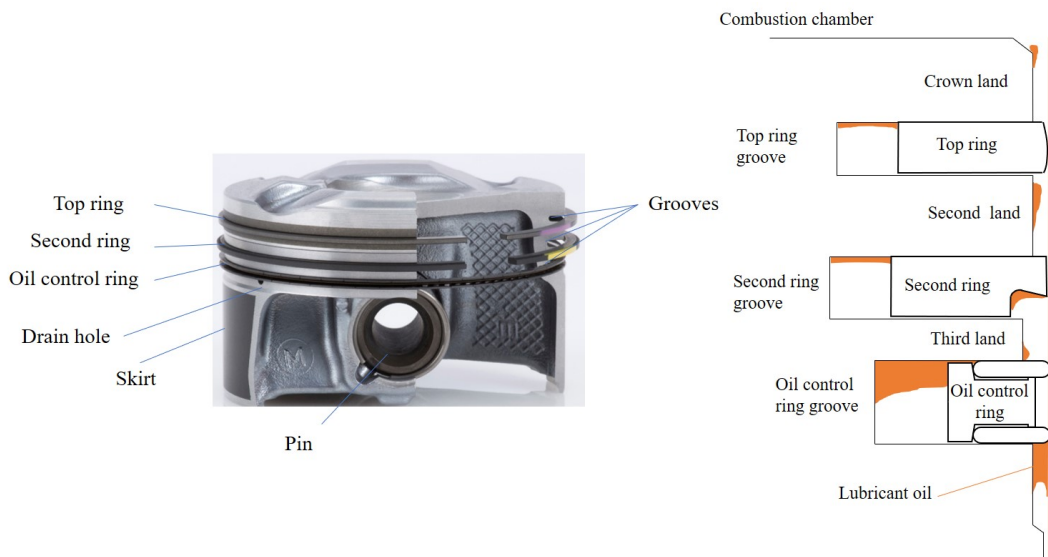
Figure 1-1: Piston Ring Pack System.

To lubricate the skirt liner interface, lubricant oil is splashed onto the liner, while

excessive oil leakage into combustion chamber may cause pollution and oil consumption. The oil control ring is mainly responsible for controlling the oil supply to top parts. Top ring, or compression ring, is directly exposed to the high pressure from combustion chamber, seals the gas leakage to minimize work loss. The second ring plays the role of both oil scraping and blowby gas control.

Compared with top two rings, oil control ring requires high tension to seal the ring liner interface and consists of multiple pieces. Twin land oil control ring, composed of a ring with two outer lands and a loaded spring, is mostly used on diesel/heavy duty engines for its robustness in more abrasive environment. Also diesel engine does not run thottled condition so twin land oil control ring gap is not vulnerable to oil leakage. Gasoline engines are mostly equipped with three-piece oil control ring (TPOCR). Upper rail, expander(or spacer) and lower rail are stacked together, as shown in figure 1-2. The expander functions as a spring, providing radial forces to two rails, thus rails can seal the liner interface. Several reasons can explain the popularity of three-piece oil control ring in gasoline engines. Firstly, the cost is cheaper than twin land oil control ring because mental forming process simplifies into coiling and gear stamping. Furthermore, the flexibility of three parts and the ear angle design of the expander allows better flank sealing which favors low load conditions in gasoline engines. Contributing the most friction among three ring and essentially playing the role of the first barrier to oil consumption, oil control ring is the most critical component in piston ring pack system.

1.3   Oil transport around TPOCR

In order to reduce the friction of rail liner interface, lubricant will be supplied from piston skirt region. To control the excessive oil and maintain a healthy ring pack system, oil control ring is mainly responsible for regulating the oil supply. Starting from the skirt area, oil may leak to groove and expander pitches through lower rail liner interface or groove flank clearance. Inside these non-contact regions including groove and expander pitches and further the piston 3rd land, oil is mostly driven
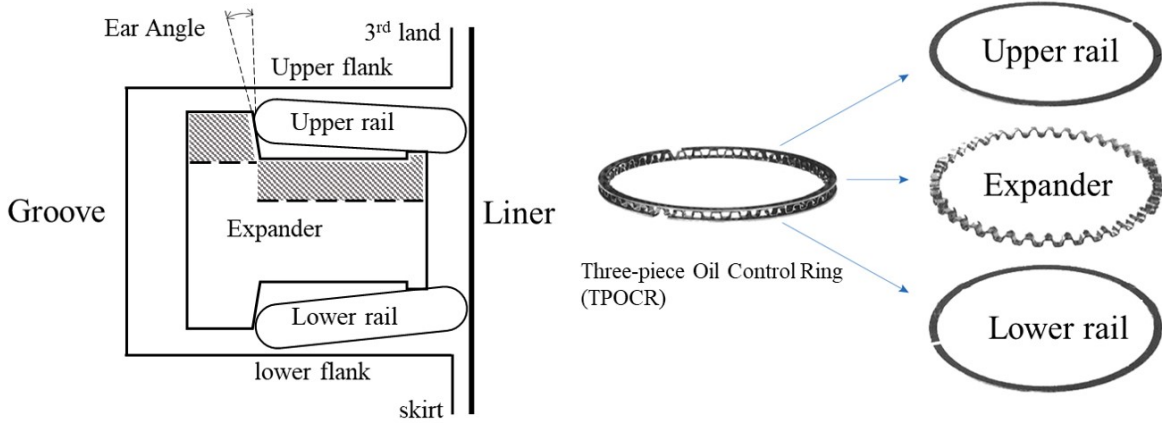
Figure 1-2: Three-piece Oil Control Ring Assembly.

by piston inertia force and gas flow effect and may leak into 3rd land through the upper rail liner clearance and groove flank clearance. Once the oil passes the OCR and reaches the piston 3rd land, step by step, it can move further upwards and potentially cause oil consumption and emission problem.

1.4 Thesis scope

This work is designed to build an effective simulation tool to predict the three-piece oil control ring dynamics integrating the oil transport, specifically on the bore-sealing, side-sealing and friction performance. The thesis will cover the modeling details and simulation results, as well as the simplification and assumptions which may require future improvements.

The second chapter starts with the ring dynamics as the model main frame. Ring dynamics set up is based on Tian's axisymmetric assumption[5], simplifying the 3D structure into 2D cross section considering the circumferential flexibility of three-piece oil control ring[7]. The detailed interaction is considered between rail and expander, rail and liner. Then it will describe the different oil transport passages including groove flank pumping, ring liner lubrication and oil movement in non-contact regions. Groove flank pumping assumes a pressure-driven oil/gas immiscible flow and is solved by finite difference method. The ring liner lubrication solves Reynolds Equation given

16

clearance profile and interface oil supply..

The third chapter will introduce a novel method to speed up physic system simulation using model order reduction (MOR) based on neural network. Ideally to integrate the oil movement in non-contact region with the other oil models, a full computational fluid dynamics (CFD) model is required to describe the oil motion. However, the expensive computational cost ($\sim$over 2 days) is not worthwhile compared with TPOCR model (5$\sim$15 minutes) thus against the original purpose of build an efficient simulation package. The treatment here is using an autoencoder neural network to extract the reduced basis in offline simulation results, and using another recurrent neural network to learn the reduced space dynamics. The non-contact oil movement in TPOCR model is running in reduced mode through these two neural networks. It is noticeable that this method is not only limited to the CFD application in this thesis, but can be extended to speed up other simulations.

In the fourth chapter, the TPOCR model is applied on a typical gasoline engine. With sample results, ring dynamics and oil transport mechanism from TPOCR model will be illustrated. The rail and expander motion dependence on engine working condition is also discussed.

In the fifth chapter, we will study a specific case by comparing the TPOCR model simulation and the 2-Dimension Laser Induced Fluorescence(2DLIF) optical engine experiments by Ahling[8]. Through a high-speed camera system with magnified view, it is possible to identify the rail motions to validate the model and collect further evidence for oil motions. With the help of TPOCR model, the detailed mechanisms behind experimental results can also be explained.

The major goal for TPOCR design optimization is the oil control performance under various working conditions. From industry experience, the gasoline engines perform well in low to intermediate working conditions, while the oil consumption increases dramatically at high load high speed condition. The sixth chapter will show further parametric study for oil transport passages discusses the potential oil consumption leakage mechanism and other engine performance considerations.

The last chapter concludes this thesis work and suggests potential future work.

Chapter 2

Model configuration

2.1 Introduction

This chapter is designed to introduce the formulation of the three-piece oil control ring model and the relationship between the rail and expander dynamics and other sub-models. As the main frame, the ring dynamics model collects the external forces such as solid contact, fluid pressure and friction forces from other sub-models and solves the rails and expander displacement with force/moment balance equations. In return, the ring dynamics model feedback clearances for the oil transport sub-models so the later could solve mass conservation equations. Among the oil sub-models, pumping model and groove oil movement are connected by mass balance and pressure boundary conditions. The groove oil movement also serves as boundary conditions for rail liner interface. In the model, bridging is considered as a binary (either flooded or dry) boundary condition because the groove oil can always flood the rail liner interface if bridging happens and the inlet pressure is negligible compared to the hydrodynamic pressure in lubrication zone.

The goal of this model is to study the three-piece oil control ring dynamics and oil control performance given engine parameters and working conditions as inputs. The model outputs:

1. rail/expander position and twist.

2. radial distribution of pressure/oil ratio through the flank clearance.

3. oil distribution on the liner .

4. forces to rail/expander

5. oil leakage/release through the pumping zone

6. oil up-scraped by rail profile

The oil up-scraped and leaked into 3rd land will potentially move to further upper regions of piston, it is used to evaluate the oil control performance of the three-piece oil control ring in this thesis.

2.2   Rails and expander dynamics

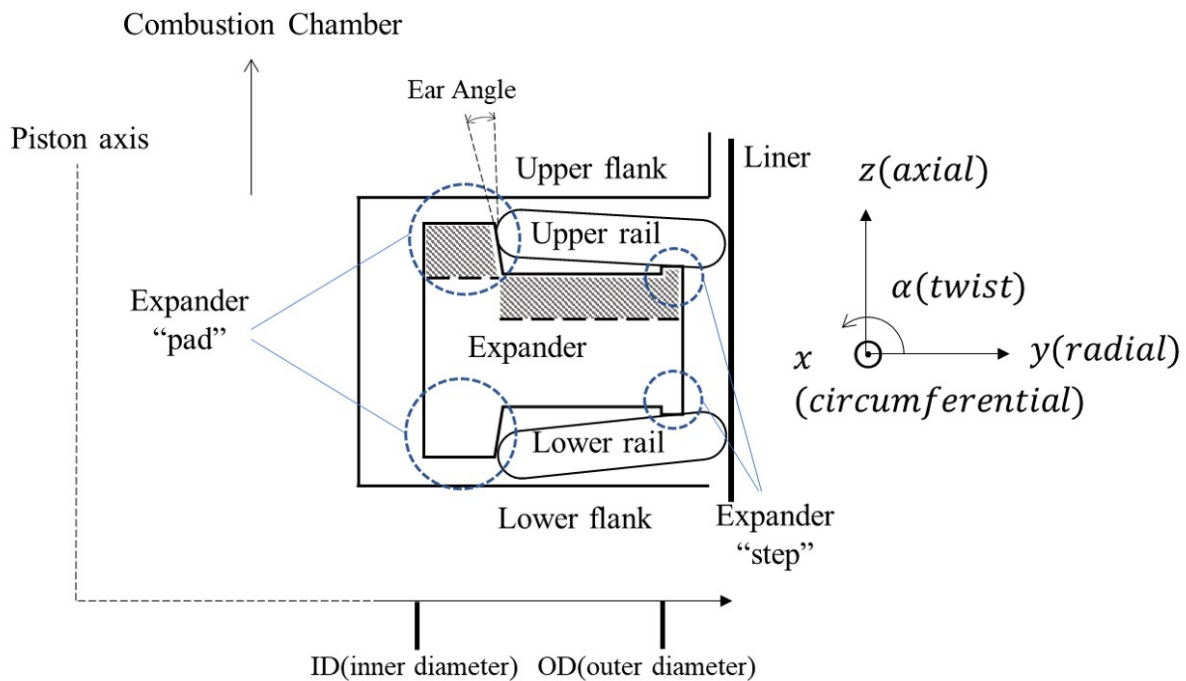Figure 2-1: Coordinate and Naming Convention for TPOCR in the Model

Figure 2-1 shows the key components in three-piece oil control ring and coordinate conventions in this thesis. In the diagram, z-direction is pointing to the combustion chamber and is also called axial direction because it is parallel to the nominal piston axis. y-direction(radial) is pointing from the piston axis to the liner and x-direction

is along the circumference. Also following the industry convention, inner diameter (ID) refers to the region relatively closer to the piston axis and outer diameter (OD) refers to the farther regions in radial direction.

In the oil control ring groove, upper and lower rails are assembled together with expander. The expander, when compressed together with the rails into the cylinder, provides tension to the rails through the contact between rail ID and "seating tab" or expander "pad" as circled out in figure 2-1. There exists an important design parameter: ear angle between the expander pad and back plane of the expander. The purpose of this design is to provide a vertical component of contact force to the rail ID so it can better seal the flank clearance. At the expander OD, there is usually a "step" as an additional design feature.

Figure 2-2: Three-piece Oil Control Ring Spacer Expander

As shown in figure 2-2, the real expander is a 3D dimension structure, the "pitches" are staggered in the circumferential direction. In the model, up and lower contact are assumed to be uniform considering the pitch distance is relatively small compared with the engine bore diameter ($\sim$roughly 50 pitches around the circumference).

In the 2D scenario, both rails and expander have three degree of freedom: y-direction (radial) displacement, z-direction displacement (axial) and twist α, which corresponds to two force and one moment balance equations.

For upper and lower rail, the equations are:

$$G_{y,i} = m_{rail}\ddot{y}_i - F_i^{liner,asp} - F_i^{liner,hydro}$$
$$- F_{y,i}^{ODgas} - F_{y,i}^{pad,asp} - F_{y,i}^{pad,fric} \tag{2.1}$$

$$G_{z,i} = m_{rail}\ddot{z}_i - F_i^{inertia} - F_i^{liner,aspfric} - F_i^{liner,hydrofric}$$
$$- F_{z,i}^{ODgas} - F_{z,i}^{pad,asp} - F_{z,i}^{pad,fric} \tag{2.2}$$
$$- F_i^{flank,pump} - F_i^{flank,asp} - F_i^{step,asp}$$

$$G_{\alpha,i} = I_{rail}\ddot{\alpha}_i - \kappa_{rail}\alpha - M_i^{liner,aspfric} - M_i^{liner,hydrofric}$$
$$- M_i^{ODgas} - M_i^{pad,asp} - M_i^{pad,fric} \tag{2.3}$$
$$- M_i^{flank,pump} - M_i^{flank,asp} - M_i^{step,asp}$$

where

m_{rail} and I_{rail} are the mass and moment of inertia of the rail.

κ_{rail} is the torsional resistance of rail.

$\ddot{y}_i$, $\ddot{z}_i$, $\ddot{\alpha}_i$ $(i = 1, 2)$ are the acceleration term of displacement and twist of two rails.

$F_i^{inertia}$ $(i = 1, 2)$ are the inertia forces of rails in the piston reference frame.

$F_i^{liner,asp}$, $F_i^{liner,aspfric}$, $M_i^{liner,aspfric}$ $(i = 1, 2)$ are the asperity contact and friction force and moment from liner to rails.

$F_i^{liner,hydro}$, $F_i^{liner,hydrofric}$, $M_i^{liner,hydrofric}$ $(i = 1, 2)$ are the hydrodynamics normal and friction force and moment from liner to rails.

$F_{y,i}^{ODgas}$, $F_{z,i}^{ODgas}$, M_i^{ODgas} $(i = 1, 2)$ are the radial, axial force and moment from 3rd land gas pressure to rails.

$F_{y,i}^{pad,asp}$, $F_{z,i}^{pad,asp}$, $M_i^{pad,asp}$ $(i = 1, 2)$ are the radial, axial force and moment from expander pad asperity contact to rails.

$F_{y,i}^{pad,fric}$, $F_{z,i}^{pad,fric}$, $M_i^{pad,fric}$ $(i = 1, 2)$ are the radial, axial force and moment from expander pad asperity friction to rails.

$F_i^{step,asp}$, $M_i^{step,asp}$ $(i = 1, 2)$ are the axial force and moment from expander step asperity contact to rails.

$F_i^{flank,pump}$, $M_i^{flank,pump}$ $(i = 1, 2)$ are the axial force and moment from groove flank

clearance pumping zone gas/oil to rails.

$F_i^{flank,asp}$, $M_i^{flank,asp}$ ($i = 1, 2$) are the axial force and moment from groove flank asperity contact to rails.

The forces applied on upper rail is shown in figure 2-3.
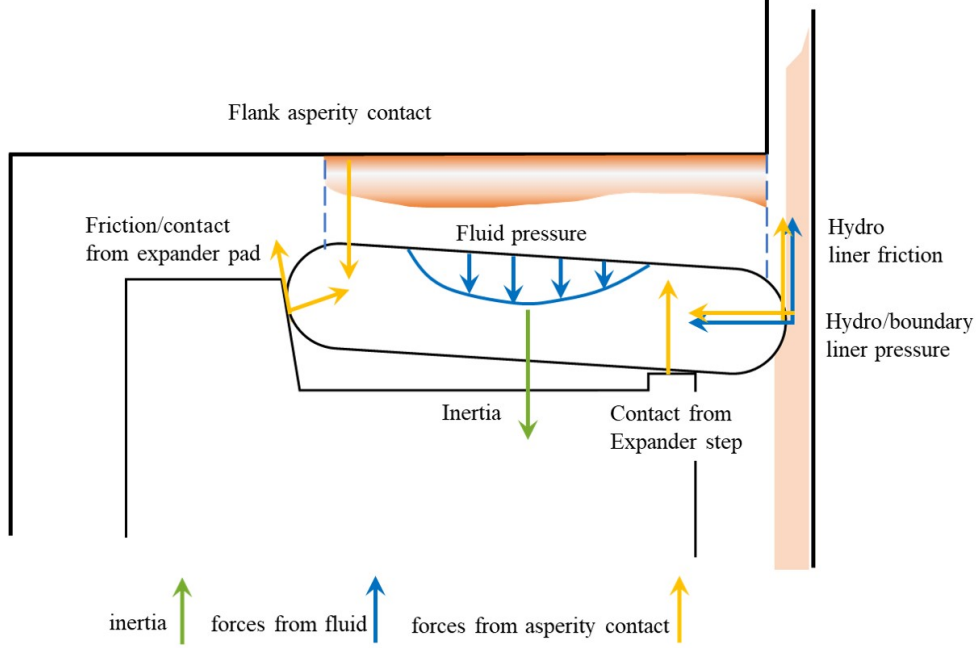
Figure 2-3: Forces to Upper Rail

For expander, the dynamics equations are:

$$G_{y,exp} = m_{exp}\ddot{y}_{exp} - F^{tension}$$
$$- \sum F_{y,i}^{rail2pad,asp} - \sum F_{y,i}^{rail2pad,fric} \tag{2.4}$$

$$G_{z,exp} = m_{exp}\ddot{z}_{exp} - F_{exp}^{inertia} - \sum F_i^{rail2step,asp}$$
$$- \sum F_{z,i}^{rail2pad,asp} - \sum F_{z,i}^{rail2pad,fric} \tag{2.5}$$

$$G_{\alpha,exp} = I_{exp}\ddot{\alpha}_{exp} - \kappa_{exp}\alpha_{exp} - \sum M_i^{rail2step,asp}$$
$$- \sum M_i^{rail2pad,asp} - \sum M_i^{rail2pad,fric} \tag{2.6}$$

where

m_{exp} and I_{exp} are the mass and moment of inertia of the expander.

κ_{exp} is the torsional resistance of expander.

23

$\ddot{y}_{exp}$, $\ddot{z}_{exp}$, $\ddot{\alpha}_{exp}$ are the acceleration term of displacement and twist of the expander.

$F^{tension}$ is the tension provided by expander.

$F^{inertia}_{exp}$ is the inertia forces of the expander in the piston reference frame.

$F^{rail2pad,asp}_{y,i}$, $F^{rail2pad,asp}_{z,i}$, $M^{rail2pad,asp}_i$ $(i = 1, 2)$ are the radial, axial force and moment from rail asperity contact to expander pad.

$F^{rail2pad,fric}_{y,i}$, $F^{rail2pad,fric}_{z,i}$, $M^{rail2pad,fric}_i$ $(i = 1, 2)$ are the radial, axial force and moment from rail asperity friction to expander pad.

$F^{rail2step,asp}_i$, $M^{rail2step,asp}_i$ $(i = 1, 2)$ are the axial force and moment from rail asperity contact to expander step.

In total, there are nine equations describing rail and expander force/moment balance.

Forces between rail and expander "step"

The interaction between expander "step" and rail OD is model as asperity contact, derived from Greenwood and Tripp theory[9] and simplified by Hu[10].

$$P_c = \begin{cases} 0 & \text{if } h \geq 4\sigma \\ P_k(4 - \frac{h}{\sigma})^z & \text{otherwise} \end{cases} \tag{2.7}$$

P_c is the local contact pressure, h is the local clearance, is the surface roughness, P_k is a pressure constant correlated by the material property of two contact surfaces and z is the constant calculated by Hu.

Forces between rail and expander "pad"

Due to the large tension of three-piece oil control ring expander, the rail ID is contacting with the expander pad all the time, otherwise the rails would malfunction without radial supporting forces. Also considering the rail ID profile will see worn shape during engine lifespan, it is difficult to determine the exact clearance between these two interfaces. In this model, it is assumed the expander tension will symmet-

24

rically distribute to upper and lower rail as radial component of the normal contact force.

During the engine cycles, the rails and expander will be dragged up and down by inertia force in the piston reference frame, it is also possible the rail and expander have relative motion along the tangential direction of the pad face. Therefore, a "slip and stick" treatment is set up for the friction and relative motion. If there is a tendency for relative motion, the two surfaces stick to each other first. After the static friction reaches the threshold, the constraint releases and dynamic friction is proportional to normal contact force by a friction coefficient. In the numerical treatment, the model reserves same slot for two equations. When two interfaces stick to each other, it is solving the geometric constraint and outputs friction. When it switches to slipping mode, friction is known and thus relative motion is allowed.

Forces between rail and groove flank

Both asperity contact and oil/gas pressure forces are considered between rail and groove. Asperity contact also utilizes the Greenwood treatment. The ring groove clearance is also a tunnel for fluid transport, when the rail squeezes the oil or leaves the flank, the fluid will pressurize or depressurize to feedback forces to rail. This phenomenon will be modeled by pumping model and is discussed in the next part.

Forces between rail and liner interface

Similar to flank interface, there exists both asperity contact and hydrodynamic forces in the rail liner interface. The asperity contact is also using the Greenwood treatment. The interface will also form a hydrodynamic lubrication layer when it reaches certain sliding velocity and there is oil supply at inlet. This will also be elaborated in the next section.

2.3 Oil transport around three-piece oil control ring

Oil transport is directly affecting the engine oil consumption, the major motivation of building the TPOCR model is to study how the oil penetrates from piston skirt to upper regions and then provide further design suggestions for a healthy system. In this model, three oil passages around oil control ring are considered: groove flank clearance pumping, rail liner lubrication and oil movement in the non-contact regions (in piston chamber and third land, behind the ring) as shown in figure 2-4.
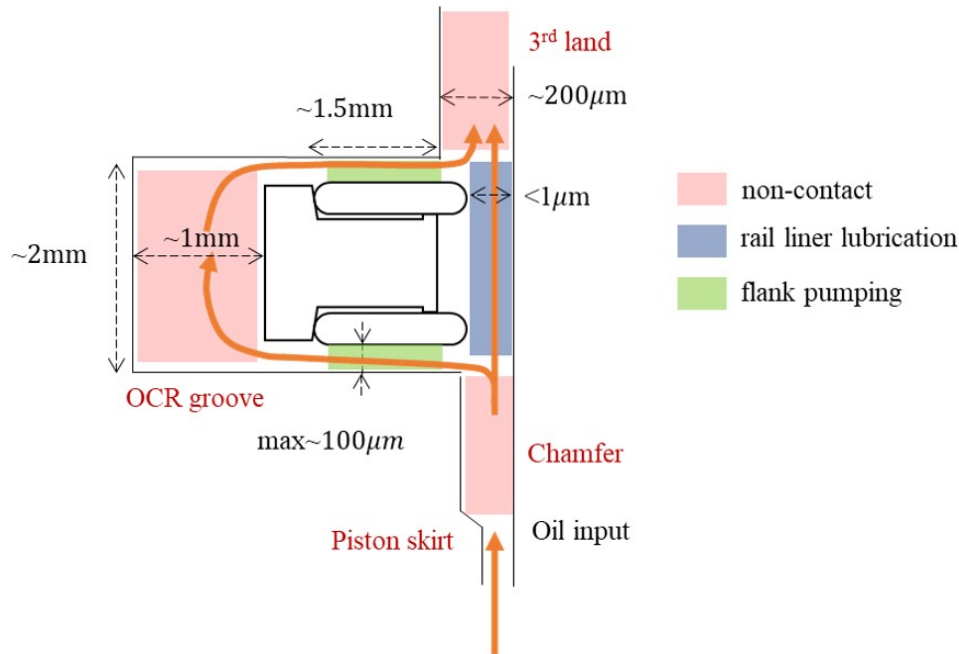
Figure 2-4: Oil Transport Zones and Scales around TPOCR

During engine cycles, piston skirt is mostly flooded by splash oil to minimize the friction power loss, this is the source of oil input into ring pack system. After oil reaches three-piece oil control ring, it is possible for oil to leak through lower rail flank clearance to the back of ring by pumping or pass the rail interface into piston third land. The oil behind oil control ring will shake up and down by piston inertia force and reach the upper rail flank clearance ID, similar to lower clearance, pumping phenomenon may transfer the oil to OD and eventually squeeze into third land.

The typical clearance for these fluid passages are also shown in the figure. For rail liner lubrication and flank pumping, the clearance scale is much smaller than

lateral length and Reynolds number is also in the laminar region (<10). It is valid to simplify the Navier-Stokes equations into pressure gradient and viscous term then use mass balance as conservation equations. In non-contact zones, thin film theory is not applicable considering the length scales. Ideally a full CFD calculation is needed to address the oil/gas motion to provide the oil/pressure boundary conditions for foregoing models. Fang[6] comprehensively applied CFD to analyze the lubricant transport in piston ring pack non-contact zones with given oil amount and fixed rail positions, it costs several hours to days for each engine cycle. This computational time is not acceptable when coupling into TPOCR model. Fang's solution is to generalize the CFD calculation into correlation with theoretical analysis, for example from the piston chamfer to lower rail OD boundary condition, given the oil supply from skirt is not affected by ring dynamics/oil amount in the groove. For the other non-contact regions, if we assume oil amount is not changing during engine cycles, it is possible to use CFD to pre-calculate the boundary conditions as inputs for TPOCR model. But this assumption without mass conservation is not necessarily true, especially when users would like to see how oil control ring groove is saturated with oil. Therefore, we introduce the method of reduced model order for CFD based on machine learning in the next chapter.

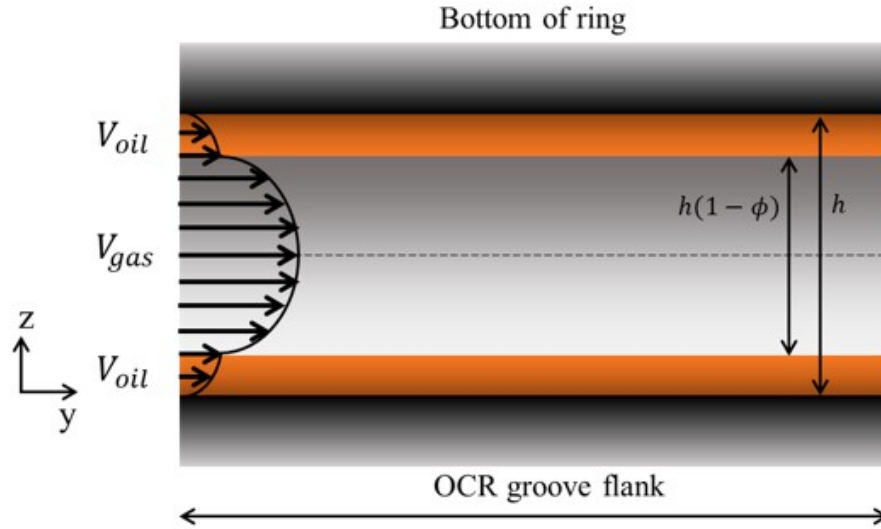## 2.3.1 Oil/gas transport (pumping) model in flank clearance

Figure 2-5: Groove Flank Clearance Oil/Gas Transport (Pumping) Model

Figure 2-5 shows the physical scenario of ring flank clearance pumping model, it is assumed oil/gas is immiscible and oil film is symmetrically distributed on both side of the clearance. Mathematically, there could be infinite possibilities how oil and gas are distributed when they coexist in the rail/groove clearance. The other more popular assumptions are 1) there are oil and gas streaks next to each other along the radial direction that are both fully contacting rail and groove flanks, 2) oil and gas are fully mixed. The first assumption is the conventional cavitation assumption in lubrication and is more valid when the oil occupation ratio is not too small. When oil occupation ratio becomes small enough such that the width of the the oil streaks is comparable with the clearance height, the oil streaks can break and the oil accumulation pattern may resemble the assumption used here. Without involving necessary physics resolving the width of the oil streaks, there are always uncertainties about the oil accumulation pattern in the partial film area. The current assumption represents perhaps the lower limit of the oil flow rate among possible patterns. Given the thin film lubrication assumption applies, the Navier-Stokes momentum equation can be simplified into viscous and pressure gradient term.

$$\frac{\partial P}{\partial y} - \mu_{oil}\frac{\partial^2 V_{y,oil}}{\partial z^2} = 0 \tag{2.8}$$

$$\frac{\partial P}{\partial y} - \mu_{gas}\frac{\partial^2 V_{y,gas}}{\partial z^2} = 0 \tag{2.9}$$

To solve the velocity profile, there are four boundary conditions, including the non-slip boundary condition at the solid surface, non-shear stress at the center line due to symmetry and velocity and shear stress continuity at the oil/gas interface.

BC1: $\qquad V_{y,oil}\Big|_{z=0} = 0 \tag{2.10}$

BC2: $\qquad \dfrac{\partial V_{y,gas}}{\partial z}\Big|_{z=h/2} = 0 \tag{2.11}$

BC3: $\qquad (V_{y,gas} - V_{y,oil})\Big|_{z=\phi h/2} = 0 \tag{2.12}$

BC4: $\qquad (\mu_{gas}\dfrac{\partial V_{y,gas}}{\partial z} - \mu_{oil}\dfrac{\partial V_{y,oil}}{\partial z})\Big|_{z=\phi h/2} = 0 \tag{2.13}$

Then we can derive the velocity profile and draw the mass conservation as the governing equations for this flank clearance pumping model:

$$\frac{\partial[(1-\phi)hP]}{\partial t} = \frac{1}{12\mu_{gas}}\frac{\partial}{\partial z}[P(1-\phi)^3 h^3 \frac{\partial P}{\partial z}] \tag{2.14}$$

$$\frac{\partial[\phi h]}{\partial t} = \frac{1}{24\mu_{oil}}\frac{\partial}{\partial z}[\phi^2(3-\phi)h^3\frac{\partial P}{\partial z}] \tag{2.15}$$

where μ_{air} and μ_{oil} are the air and oil viscosity, h, ϕ and P are the local clearance, oil ratio and pressure respectively.

In practice, TPOCR model numerically solves these two equations. 10-20 cells
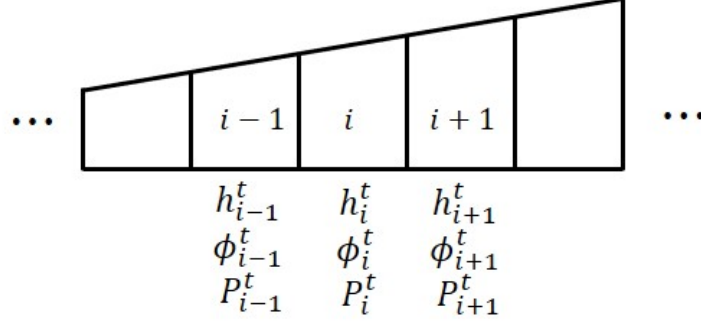
Figure 2-6: Upwind Scheme

are suggested for acceptible accuracy and efficiency. To guarantee the stability of equations, upwind scheme is used for the convection terms as shown in figure 2-6. In the finite different method, the unknown locates at the center of each cell marked by i and t as spacial and temporal index respectively. The discretized equations are as following:

$$\frac{(1 - \phi_i^t)h_i^t P_i^t - (1 - \phi_i^{t-1})h_i^{t-1} P_i^{t-1}}{\Delta t}$$
$$= \frac{1}{12\mu_{gas}}\frac{1}{\Delta z}[P_{i+0.5}^t(1 - \phi_{i+0.5}^t)^3(h_{i+0.5}^t)^3\frac{P_{i+1}^t - P_i^t}{\Delta z}$$
$$- P_{i-0.5}^t(1 - \phi_{i-0.5}^t)^3(h_{i-0.5}^t)^3\frac{P_i^t - P_{i-1}^t}{\Delta z}] \tag{2.16}$$

$$\frac{\phi_i^t h_i^t - \phi_i^{t-1} h_i^{t-1}}{\Delta t}$$
$$= \frac{1}{24\mu_{oil}}\frac{1}{\Delta z}[\phi_{i+0.5}^t{}^2(3 - \phi_{i+0.5}^t)(h_{i+0.5}^t)^3\frac{P_{i+1}^t - P_i^t}{\Delta z}$$
$$- \phi_{i-0.5}^t{}^2(3 - \phi_{i-0.5}^t)(h_{i-0.5}^t)^3\frac{P_i^t - P_{i-1}^t}{\Delta z}] \tag{2.17}$$

where index $i \pm 0.5$ indicates the value on the cell boundary dependent on the direction of flow:

$$\phi_{i-0.5}, P_{i-0.5} = \begin{cases} \phi_i, P_i & \text{if } P_i \geq P_{i-1} \\ \phi_{i-1}, P_{i-1} & \text{otherwise} \end{cases} \tag{2.18}$$

30

$$\phi_{i+0.5}, P_{i+0.5} = \begin{cases} \phi_{i+1}, P_{i+1} & \text{if } P_{i+1} \geq P_i \\ \phi_i, P_i & \text{otherwise} \end{cases} \tag{2.19}$$

2.3.2 Rail liner lubrication
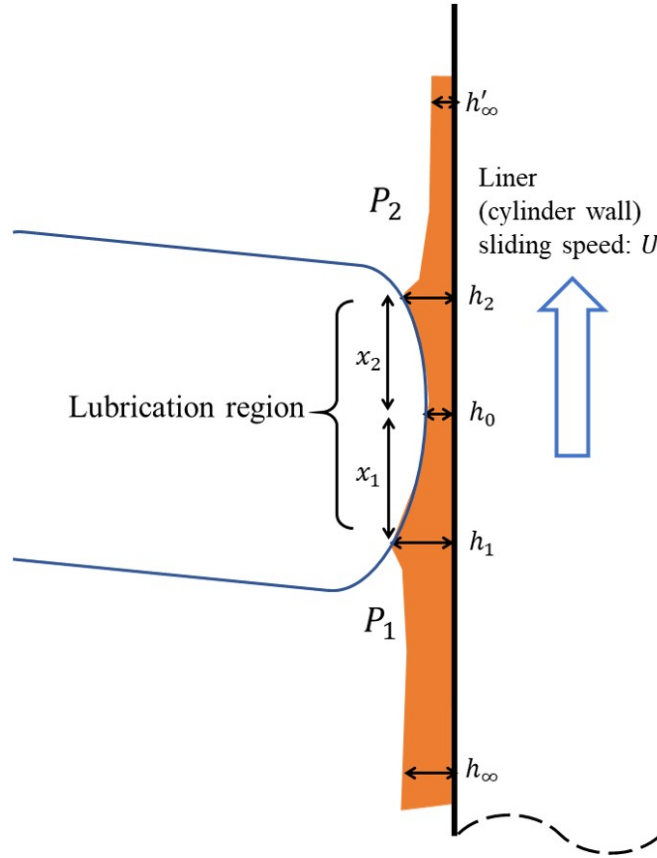
Figure 2-7: Rail Liner Lubrication Model

The purpose of rail liner lubrication model, as shown in figure 2-7, is to calculate the hydrodynamic forces from liner oil to rail and remaining oil film thickness h'_∞ after rail pass, given the rail/liner relative position and leading edge oil h_∞ as known inputs.

The inlet oil starts to attach to rail profile at x_1 and detaches at x_2, the wetting area between x_1 to x_2 is defined as lubrication region. Reynolds exit condition is used to x_2:

$$\left. \frac{\partial P}{\partial x} \right|_{x=x_2} = 0 \tag{2.20}$$

Then the steady state Reynolds equation can be written as:

$$\frac{dP}{dx} = \frac{6\mu U}{h(x)^3}(h(x) - h(x_2)) \tag{2.21}$$

And the trailing oil film thickness is exactly half of (x_2) by flow rate mass conservation:

$$h(x_2) = 2h'_\infty \tag{2.22}$$

Neglecting the pressure difference between inlet and outlet due to the fact oil control ring groove pressure is close to atmosphere, we have:

$$0 = P_2 - P_1 = \int_{x_1}^{x_2} \frac{dP}{dx} dx = \int_{x_1}^{x_2} \frac{6\mu U}{h(x)^3}(h(x) - h(x_2)) dx \tag{2.23}$$

There established a dependency between x_1 and x_2. Once the leading edge oil film thickness is known, it is possible to solve the trailing edge oil film thickness by Equation 2.23. In model implementation, the liner is equally divided into 1000 sections to track the oil film thickness left on the liner. The leading edge oil film thickness can be extracted from the oil distribution and later it will be updated after rail passes. Besides, the lower rail is always assumed to be fully flooded in down stroke considering skirt oil and additional bridging time input may be used for upper rail inlet oil.

The hydrodynamic pressure from oil to rail can be integrated from:

$$f_{hydro} = \int_{x_1}^{x_2} P dx \tag{2.24}$$

Liu[11] and Li developed an correlation for the pressure based on numerical results for parabolic rail profile:

$$f_{hydro} = \frac{12\mu V}{a/h_0} c \left(\frac{1 + tanh(\frac{log_{10}(ax_1^2/h_0)+d}{e})}{2} \right)^b \tag{2.25}$$

where h_0 is the minimum clearance between the rail profile and the liner and x_1 is the leading edge wetting length, as shown in figure 2-7. The term of a is the ring

32

profile shape factor and b, c, d, e are universal constants.

2.4 3rd land pressure calculation

The 3rd land pressure is important for both rail dynamics and oil transport. In the simulation package, the 3rd land pressure can be imported from measurement or estimated from blowby gas. For the ring pack model, the blowby rate is mostly controlled by the top ring, it is reasonable to decouple the top 2 ring gas flow with OCR model. While when calculating the 3rd land pressure, the TPOCR motion is critical since the the clearance determines the leakage through the upper groove. The TPOCR model imports the gas flow from 2nd land zone to 3rd land as an input, this flow is predicted from Tian's 2D ring pack model[4]. The configuration for 3rd land pressure calculation is shown in figure 2-8.
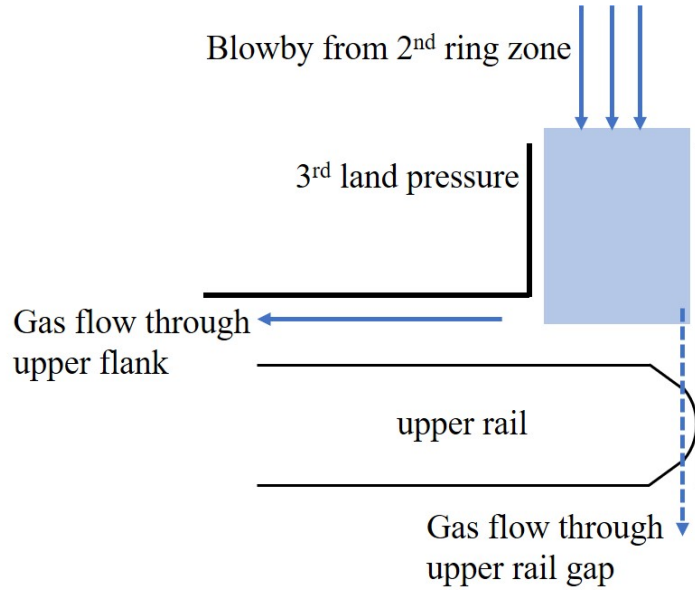

Figure 2-8: 3rd Land Pressure Calculation

The mass balance equation for 3rd land pressure is:

$$\frac{1}{RT}\frac{d(PV)}{dt} = \dot{m}_{2ndringzone} - \dot{m}_{upperflank} - \dot{m}_{TPOCRgap} \tag{2.26}$$

where R,T,P,V are the 3rd land specific gas constant, temperature, pressure and

volume respectively. $\dot{m}_{2ndringzone}$ is the inputs from gas flow from 2nd ring zone, $\dot{m}_{upperflank}$ is the gas flow from upper flank pumping and $\dot{m}_{TPOCRgap}$ is the gas flow through TPOCR upper rail gap.

2.5 Computation Algorithm

The TPOCR model is solving a multi-physics system, including the rail dynamics, oil and gas transport. The rail weight is very light compared with its surrounding forces, a global implicit scheme is needed for the stiff set of equations. There are nine equations for the rail/expander dynamics, two for pad slip-stick conditions and one for 3rd land mass conservation, corresponding to 12 unknowns here. There are roughly 100 equations/unknowns for pumping oil/gas mass conservations depending on the mesh size, which is relatively large. To facilitate the development process and minimize the change for human error, numerical Jacobian matrix is used for the first 12 unknowns. Pumping equation derivatives are resolved by analytical Jacobian matrix for efficiency. Figure 2-9 is the structure of the hybrid Jacobian matrix.
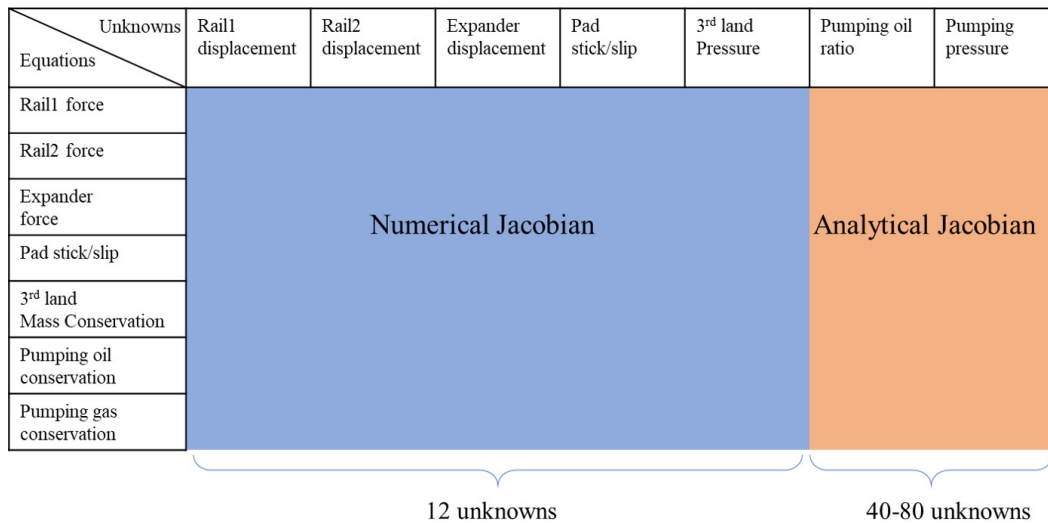

Figure 2-9: Hybrid Jacobian

During iterations of Newton-Raphson method, a line-search method is used by approximating error as a parabolic function. This method speeds up the convergence and prevents overshooting.

Chapter 3

Reduced order model of groove oil movement based on autoencoder

3.1 Introduction

The purpose of building the TPOCR model is to evaluate the system performance with decent accuracy and computational efficiency, by reducing a complex physical system into smaller space. For instance, using 2D description to represent 3D structure is a traditional technique of modeling by simplifying the system from physics understanding. In the TPOCR model, the oil movement inside groove and expander is critical to rail dynamics and other oil transport models, while it usually requires heavy computation for acceptable accuracy. As a comparison, the TPOCR main model costs less than 5 minutes for two engine cycles on a 3700x AMD CPU with single thread mode and memory usage is less than 20MB. For the standard CFD calculation of groove oil movement, it usually costs a few days and occupies gigabytes of memory, thus it is impractical to couple the full CFD model into the system. The easy treatment is to decouple the CFD with TPOCR model, assuming the oil volume is not changing significantly within certain cycles and CFD computation domain is not affected by the sub-models from TPOCR. These assumptions may not always be valid, for example, if we are exploring a balanced state of oil amount in the groove. In this case, a reduced model for fluids in numerical point of view should be introduced

to couple with the TPOCR model.

Model order reduction (MOR), generally referring to the numerical method of mapping a large-scale model into a much smaller space, is another technique to speed up the full model with lower order approximation. There are mainly two steps in MOR implementation, first step is to find a reduced space basis for full space, second is to map the original governing equations to the reduced space. Assuming full space representation x has dimension of n and reduced space representation x_r has dimension of q. Note that in order to speed up calculation, both reduced space representation and operation complexity should correspond to a small number q. To find out the projection space V, commonly used methods include Proper orthogonal decomposition(POD)/singular value decomposition(SVD), modal analysis(eigenvalues), moment based methods, Krylov space methods, etc. These methods project the full space x into the reduced space x_r through linear combination of reduced space $x \approx V x_r$, if the original governing equation is in a linear form such as $\dot{x} = Ax + b$ where A is a constant matrix and b is the source term, and the reduce space basis are orthogonal and normalized, it is possible to rewrite the equation into:

$$
\begin{aligned}
\dot{x}_r = V^{-1} V \dot{x}_r &\approx V^{-1} \dot{x} \\
&= V^{-1}(Ax - b) = V^{-1} A V \dot{x}_r + V^{-1} b \\
&= A_r \dot{x}_r + b_r
\end{aligned}
\tag{3.1}
$$

where $A_r = V^{-1} A V$ and b_r are the operators in the reduced space with size q, then the equation downgrades into $\dot{x}_r = A_r \dot{x}_r + b_r$ with both unknowns and operation complexity on the order of q.

With proper implementation on a proper system, these methods usually reduce calculation time by orders of magnitude with the minor cost of losing quantitatively controlled accuracy. Despite its performance, MOR is not a universal solution due to a few limitations of models. Firstly, the model shall be reducible into some sub-space,

this is generally true if we can tell certain "patterns" of the full model. Secondly, the physical system requires high linearity either on projection or equations. Otherwise, piecewise MORs are needed to capture the nonlinear behaviors. If the equations have polynomial terms, it is also possible to formulate a reduced order model with kronecker product representation[12]. However, the fluid motions is rather complicated, even for a simple case when groove oil is shaking up and down in the as showed in figure 3-1. If we decompose the CFD snapshots with SVD, the singular values are not decaying fast, which means low rank linear representation will be inaccurate considering the error is bounded by a large remaining singular value.
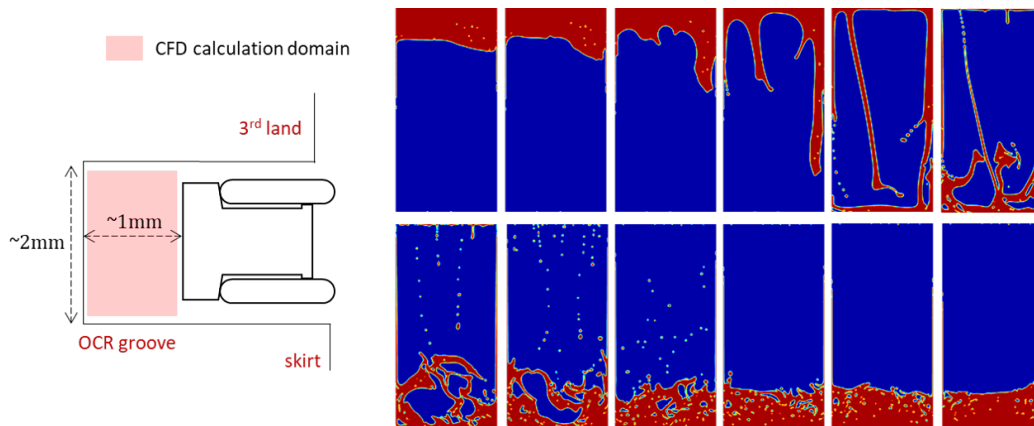

Figure 3-1: Snapshots of Groove Oil CFD Results

Thus, we introduce autoencoder as a tool to decompose the system into smaller space with nonlinear representation. The basic architecture of a vanilla autoencoder is shown in figure 3-2, it is a special feedforward multilayer perceptron (MLP) neural network same number of neurons in input and output. In the middle of the neural network, there lies a "bottleneck" for the code. The encoder compresses the input into code and decoder reconstructs the input, the loss function is usually set to be the distance between original input and output. Essentially the code is a low rank representation of the full space, the non-linearity in the neural network provides additional complexity for both coding processes.

While one should also be cautious when expanding the size of neural network, over-fitting will be a problem with unnecessary model capacity. There is another
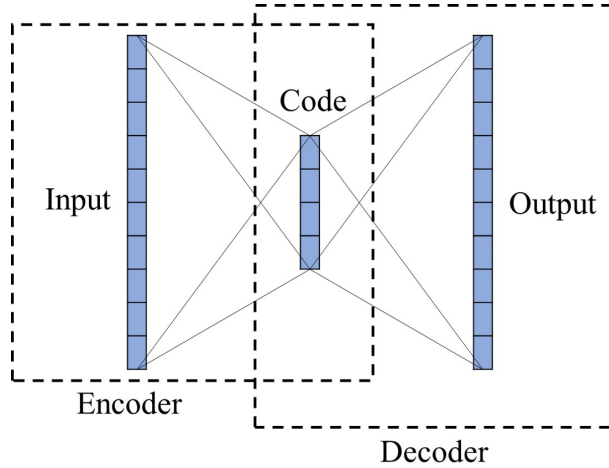
Figure 3-2: Autoencoder

concern regarding the non-contiguous basis of the vanilla autoencoder, the reduced basis may cluster in different zones and leave meaningless areas in the middle. With deterministic feed-forward procedure, it is possible to draw illogical output from the gap. To resolve this issue, there is a rising popularity in a special kind of autoencoder called variational autoencoder (VAE)[13]. In the VAE, the latent variable or the reduced space z is assumed to have a family of distributions, which we assume it follows Gaussian in the CFD case. The encoder part correlates the input into a vector of mean μ and variance σ for the distribution, in the decoder part the latent variable is sampled from the distribution and proceed in the layers into output. The major advantage of the sampling process helps improve the interpretability of the surrounding area of the basis.

Now suppose the complex CFD simulations can be reduced into a smaller size. The second step will be mapping the CFD governing equations to the reduce space. Given the model capacity of neural network, it is also possible to learn the reduce space state equations, or its trajectory dependence of other physical inputs such as gravity as a function of time in the CFD case. Besides the full driven method, other physical constraint like mass/momentum conservation can be applied into either autoencoder part or reduce space state equations as a loss function. In this chapter, detailed implementation of MOR method based on neural networks will be applied to speed
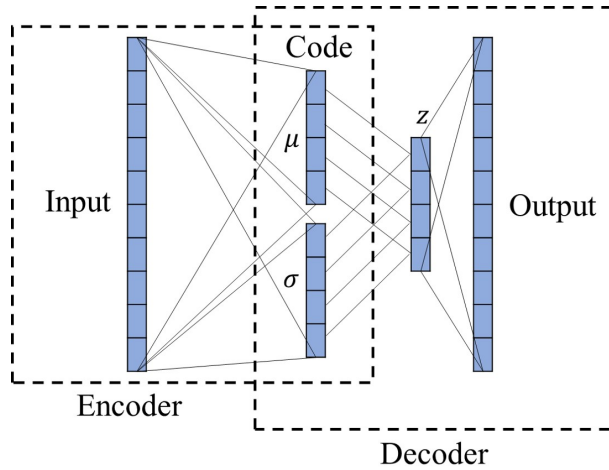
Figure 3-3: Variantional Autoencoder

up the CFD calculation. First neural networks is used to reduce the model order, then second neural network learns the dynamics of reduce space.

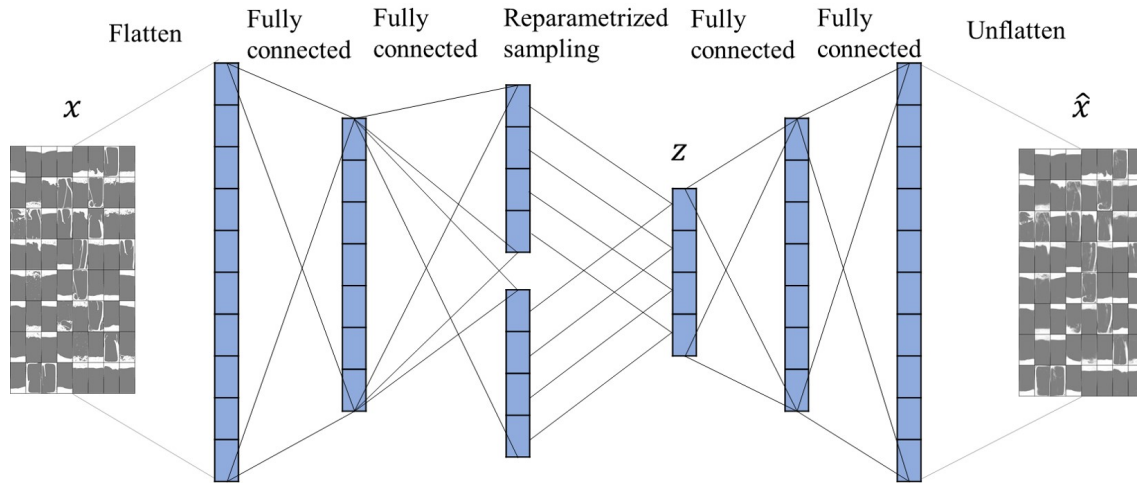## 3.2 Low order representation of CFD results by VAE

Figure 3-4: Variantional Autoencoder Configuration

Figure 3-4 shows the structure of VAE for oil ratio distributions. Both encoder and decoder part consist of one hidden layer with 128 neurons and the reduced space in the middle has dimension of 4. The batch input is randomly selected from the snapshots of the CFD results, each snapshot is a 200 by 100 image oil distribution.

If we denote original inputs is x and reconstructed output is $\hat{x}$. .The loss function for the autoencoder is written as:

$$loss = \text{mean square error}(\hat{x}, x) + D_{\text{KL}}\left(Q(z)||N(0,1)\right) + \text{physics constraints} \quad (3.2)$$

where D_{KL} denotes the Kullback–Leibler divergence (KL divergence), $Q(z)$ is the Gaussian distribution encoded by the encoder and $N(0,1)$ is the standard Gaussian distribution. Intuitively the first term captures how close the reconstructed input is to the original input and second term is penalizing the latent space distribution deviating from Gaussian. While from the variational inference perspective the loss can be also viewed as the distance between conditional probability of latent space given inputs against our choice of $Q(z)$ from the normal distribution family. The last term is to regularize the physics constraint in the system, here we use mass conservation for the oil distribution.

Figure 3-5 shows the comparison of randomly chosen snapshots of oil distribution and reconstructed results from VAE. VAE is qualitatively capable to reconstruct the major pattern of original information with a compressed space of 4 dimensions. While in the current setup, some details are missing, like the liquid droplets and fluids may not be continuous. Considering the TPOCR model is more interested in the timing when oil reaches and leaves corner, it is acceptable to neglect these details at this stage. If in the future if users are more sensitive in other features, it is possible to force additional physical constraints such as mass conservation.
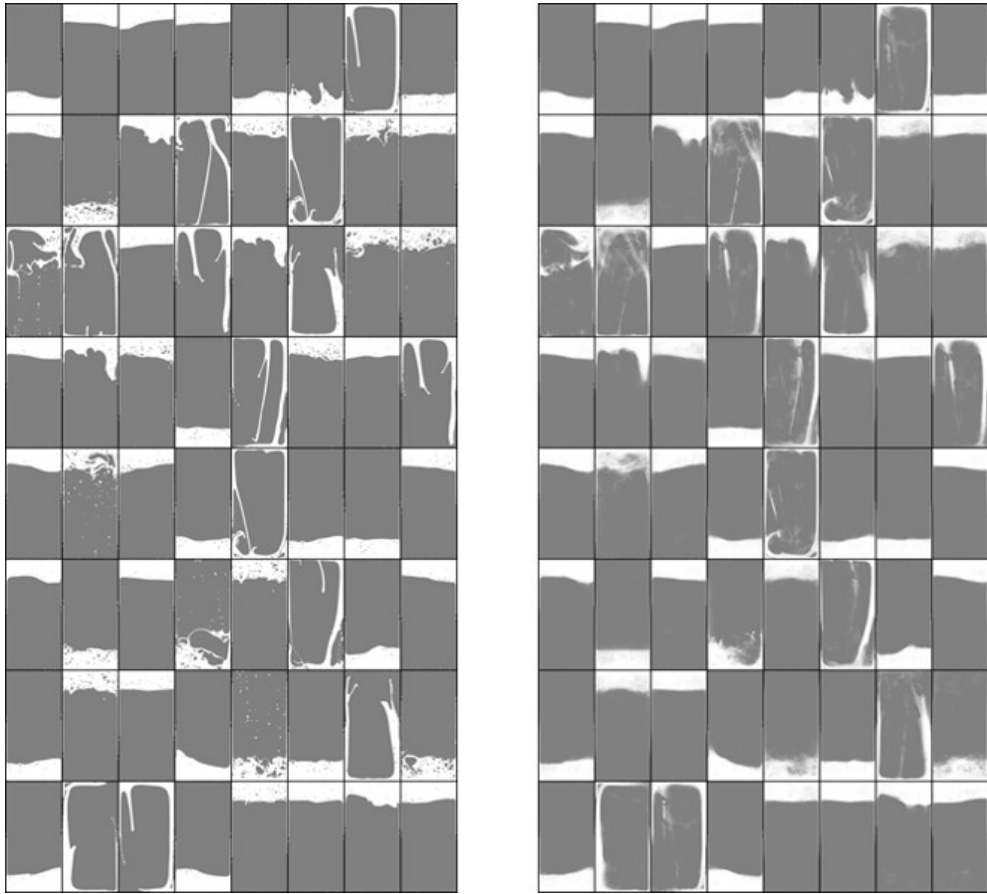
Figure 3-5: Snapshots of Groove Oil and Reconstruction from VAE

3.3   Recurrent neural network

The transient dynamics of oil motion inside the groove is a time marching physical system described by Navier-Stokes equations and volume of fluid method (VOF) on the oil/gas interface. Conventional CFD methods solves these governing equations by discretization on the spatial and temporal domain. In the reduced order dynamics, considering only oil volume data is captured, the information of at least two past times needs to be involved to predict the future state. While more time steps may be needed to resolve transient process such as pressure drop on the fluid wall boundary. Instead of applying a hyperparameter of how many steps to trace back, we can take advantage of the recurrent neural network (RNN) with hidden state automatically recognizing which states are needed from past.
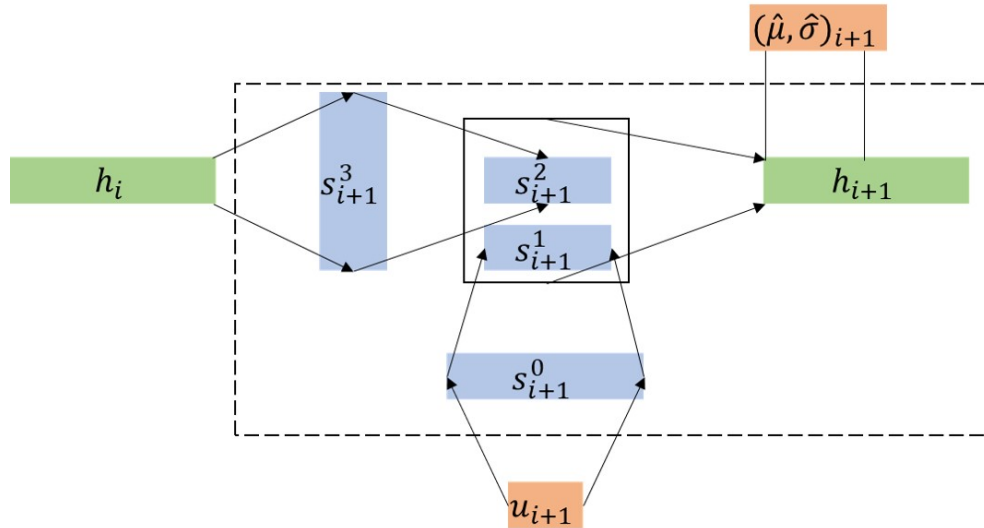

Figure 3-6: Recurrent Neural Network Configuration

Figure 3-6 shows the configuration of the RNN cell for reduce order dynamics with color boxes representing vectors, where i is the step index, h is the hidden state with size 20, u is the input for each time step, s are the intermediate hidden layers. Each arrow here represents a fully connect layer operation and the solid square box represents concatenating two vectors. Output $(\hat{\mu}, \hat{\sigma})$ is directly truncated from the hidden state h. Specifically in the oil transfer model, input u is gravity in piston reference as a time dependent variable and output $(\hat{\mu}, \hat{\sigma})$ is the distribution of reduce

representation of oil. This RNN cell is a variation of vanilla RNN with a few hidden layers in the cell. There are a few reasons to use this structure. Firstly, the output inherits in the hidden layer thus there exists a direct mapping between the output and hidden state. This is convenient to couple with other models, for instance, if we want to add oil into this model, we can decode the output back into the full space, force extra oil then encode back to the reduce space. Secondly, the general structure is inspired by the vanilla RNN instead of more popular Long Short Term Memory networks (LSTM) because from previous experience the recent a few steps are more critical to fluid dynamics so there is no need for long term memory. Thirdly, extra fully connected layers increase the model capacity of vanilla RNN so model is capable to fit the data set.

3.4   Sample Results

Figure 3-7 shows the time series snapshots of oil movement when piston approaches bottom dead center and inertia drags oil from top to bottom. The upper row is the CFD results for 400 time steps and lower row is the comparison from MOR results. The engine speed is 3000rpm and each time step is 2e-5 second. The TPOCR model is mostly interested in the timing when oil reaches the upper and lower right corner, the MOR results showed descent approximation for the bulk oil up and down motions.

The output of this MOR method will serve as the groove side boundary conditions for pumping models in the TPOCR model, to predict the oil leakage through flank clearance.

By the time of thesis completion, the autoencoder cannot handle significant amount of oil addition to the groove due to the training data representation. In the future, more CFD data is required for accommodating to various oil amount to build a fully mass conservation oil transport around TPOCR.

The overall idea of this method is to use autoencoder to reduce the physical system and another neural network to learn the dynamics equations in the reduce space. This allows the neural network gain additional interpretability from physics

perspective and the reduced model takes advantage of non-linear properties of neural network. With the flexibility of loss function choice, this method could handle data or physics driven learning methods.

In the implementation, the stability may be an issue when the RNN is not comfortable with the time sequence input such as gravity in this CFD case. This raises the interest for regulating the stability of RNN as a dynamic system in the future work.
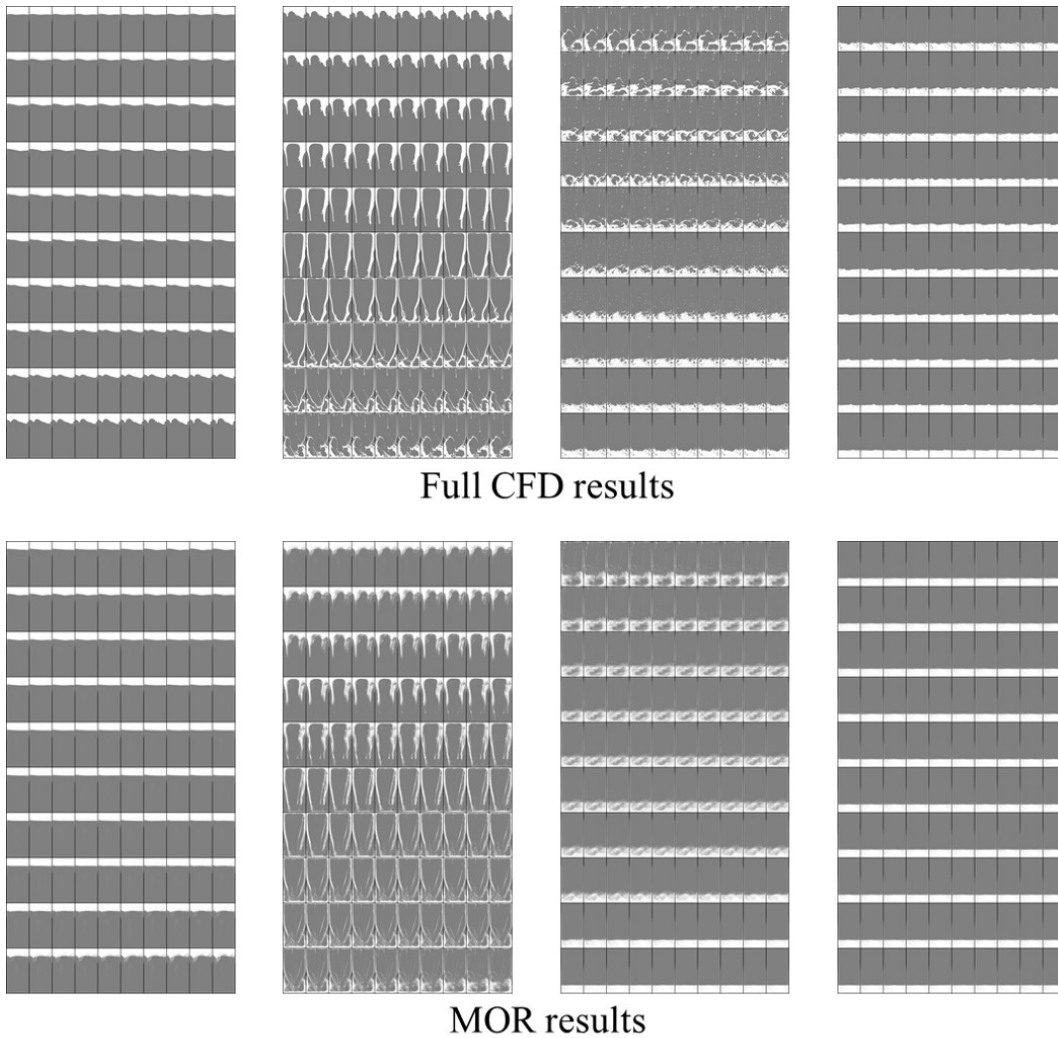

Figure 3-7: MOR Sample Results

44

Chapter 4

Model Application on a gasoline engine

4.1 Introduction

Despite the long history of application and research, the internal combustion engine industry and academia still lack the understanding of oil transport mechanism in the piston ring pack. From previous experiences, oil consumption is strongly favoring high speed and high load working conditions on gasoline engines with three-piece oil control ring (TPOCR). In engine operations, the piston inertia is proportional to the square of engine speed. The ear angle design is supposed to seal the rail flank clearance. At high speed, the rail dynamics is more less inertia-dominant, this may open rail groove clearance for potential oil leakage. Besides, groove oil bridging happens more frequently at high load high speed engine conditions, feeding additional oil to rail liner lubrication inlet and causing up-scraping. All these unknowns or guesses raised the interest for a comprehensive analysis based on the TPOCR model, to quantitatively study the manner of oil transport and figure out the dominant factors determining the system performance.

In this chapter, the TPOCR model is applied on a typical gasoline engine. A sample result is used to illustrate the outputs and oil leakage mechanisms. A general trend of rail motion in terms of working conditions.

4.2 Sample results

The model is first applied to an experimental single cylinder engine with $\sim 80mm$ bore and $\sim 90mm$ stroke. This engine is set up with laser induced fluorescence cameras(2DLIF) to capture the high speed, high resolution pictures of oil and rail motions.

The operation condition chosen for baseline result is 5000rpm/700mBar intake pressure. At this engine speed, rails will be lifted due to high inertia. Upper rail motions will differ between intake/compression stroke with combustion/exhaust stroke due to 3rd land pressure.

Driving forces

In this thesis, all the dynamics are referenced to the piston. When the piston is reciprocating during the engine cycle, its relative motion with liner and absolute acceleration are shown as in figure 4-1(inertia here is the opposite of acceleration). There are the causes for two major driving forces for rail/expander motions: liner friction and inertia force. In the piston down stroke, liner friction to rail is positive(pointing to the combustion chamber) and vice versa for up stroke. The inertia force is pointing positive when piston approaches top dead center (TDC) and turns negative around bottom dead center (BDC). Notice piston motion is not a perfect sinusoid due to the slider-crank kinematics, absolute value of inertia around TDC is greater than BDC.

Rail dynamics

Figure 4-2 shows the predicted flank clearance for upper and lower rail throughout one engine cycle. In this thesis, 90°CA denotes the combustion TDC and ±360°CA are intake TDC.

From beginning of intake stroke, inertia force initially points upwards, upper rail is pushed to the groove flank and lower rail is lifted. Lower rail returns flank when piston approaches BDC, but upper rail still sticks to top due to the suction force from pumping, although inertia force already changes direction. Right after −180°CA, when piston velocity shifts direction and so does the liner friction, the total external
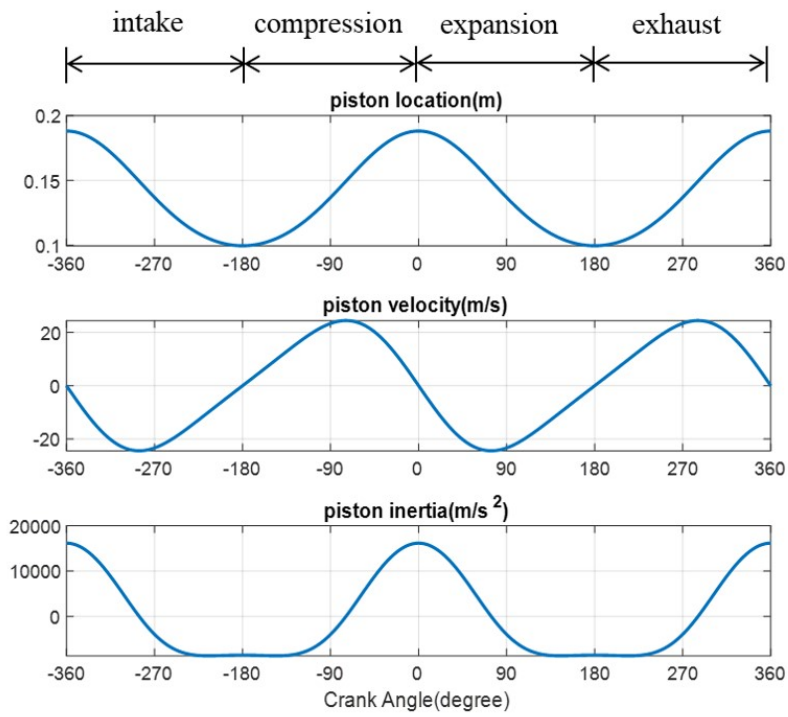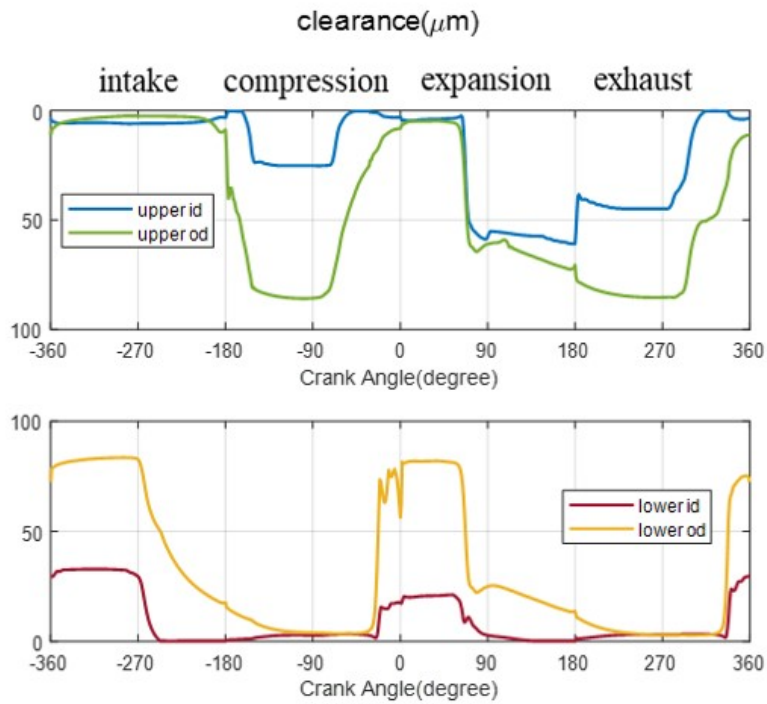
46

Figure 4-1: Piston Kinematics

Figure 4-2: Rail Groove Flank Clearance

force on rail is able to lift the upper rail clearance. In the expansion stroke, the upper rail lifts earlier than in the intake stroke, this is because the rail OD is facing a higher 3rd land pressure. For lower rail, the rail motions are similar between intake/compression and expansion/exhaust because the groove pressure is close to atmosphere. Six snapshots of rail motions at different crank angles are shown in figure 4-3.
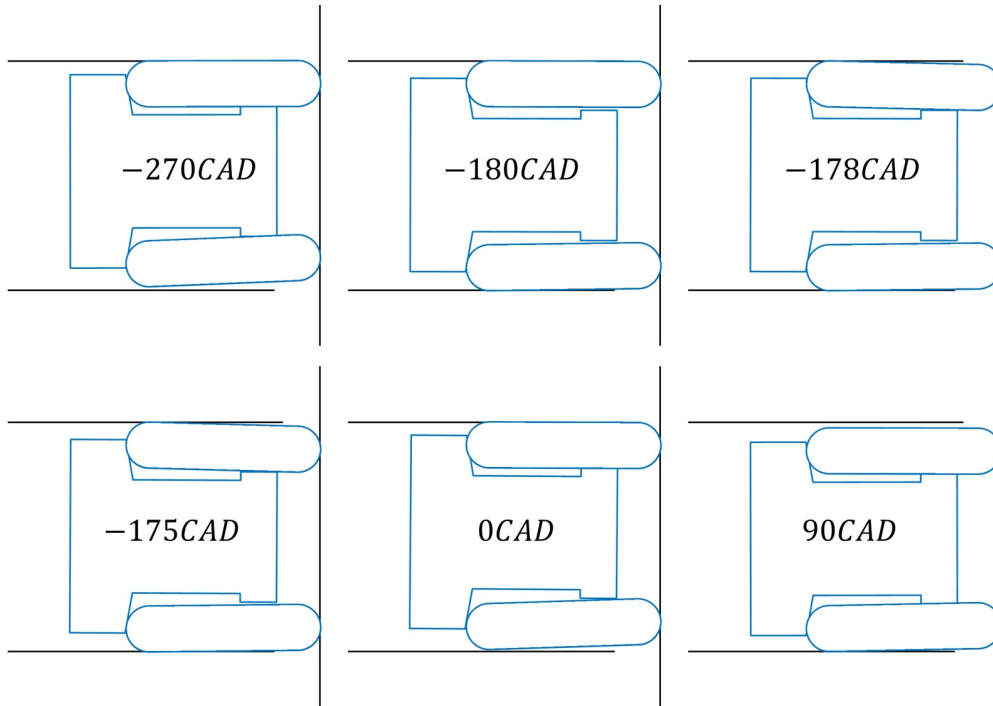

Figure 4-3: 6 Snapshots of TPOCR Motions(rail ID and OD profile not in shape)

Forces on rail

Figure 4-4 shows the all the radial and axial forces to upper rail throughout one engine cycle. The axial force figure clearly shows the OD gas pressure differs between intake and expansion. Pumping pressure has a large negative peak around BDC, meaning the squeezed oil in upper groove clearance supports the inertia force of all three pieces. It is worth noticing that pumping force also has a positive fraction around $-180°$CA. This is when inertia is trying to pull the rail from clearance, the oil inside the clearance will generate a negative pressure due to impressibility to suck the rail back to flank.

In the radial force figure, the rail component of rail-pad contact is essentially from the expander tension. Around TDC/BDC, when piston velocity is very low, rail liner asperity contacts balance most of the radial forces. During mid stroke, hydrodynamic lubrication will build a supporting pressure playing a more important role.
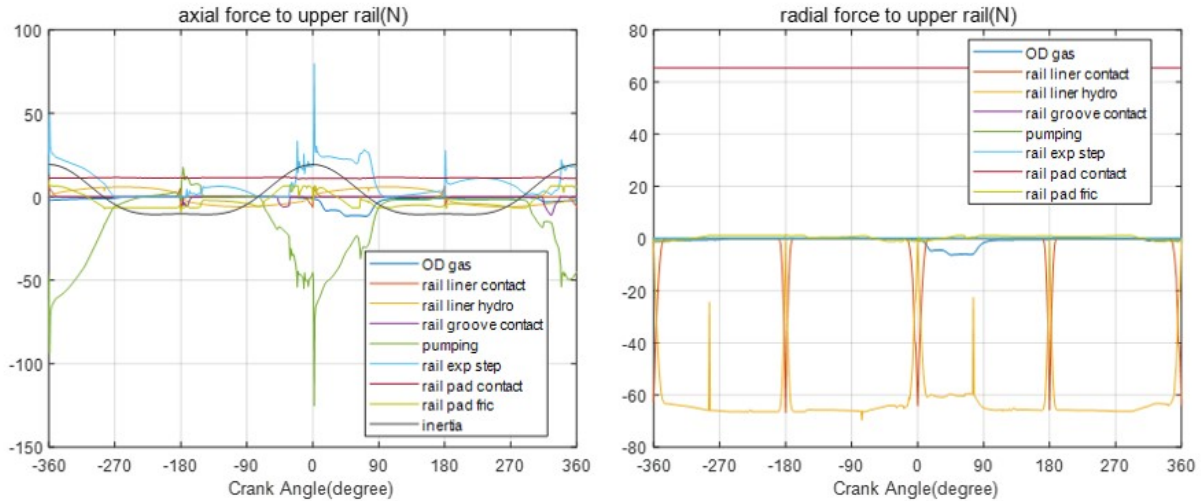

Figure 4-4: Radial and Axial Forces to Upper Rail

Rail groove pumping

As stated in the above paragraph, rail groove pumping is one of the major reaction forces to alleviate the dramatic external driving force to the light rings, while its behavior is different between suction and squeezing. In the operating piston oil control ring groove, the oil viscosity is roughly 2-3 orders of magnitude larger than the air, and oil is assumed incompressible but air can be modelled as ideal gas. These property differences allow air to flow much faster than the oil.

Figure 4-5 shows the clearance, oil thickness (orange part) and pressure distribution during the squeezing process when upper rail hits the flank. At $-90°$CA, pressure along the pumping area is at ambient pressure and there is some air bubble at ID. As the rail starts pushing the liquid, pressure will raise and the air bubble is squeezed out of ID and later the clearance is filled with oil.

Figure 4-6 shows the opposite scenario when rail leaves the flank and clearance opens. At $-180°$CA, rail sits at the top of groove and clearance is on the surface
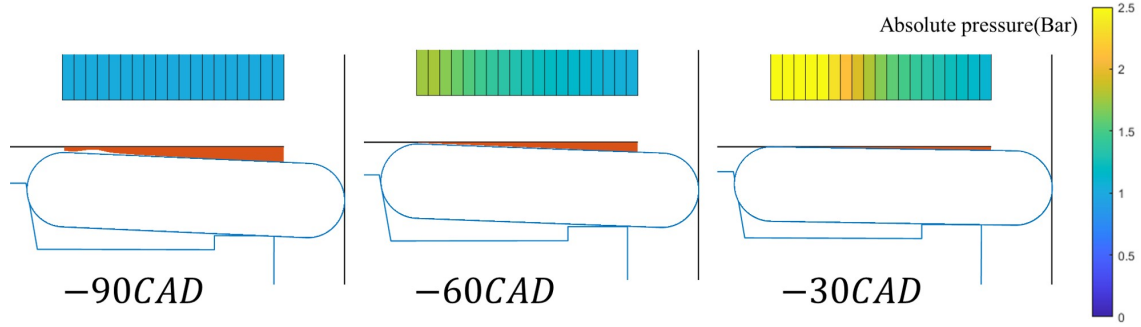
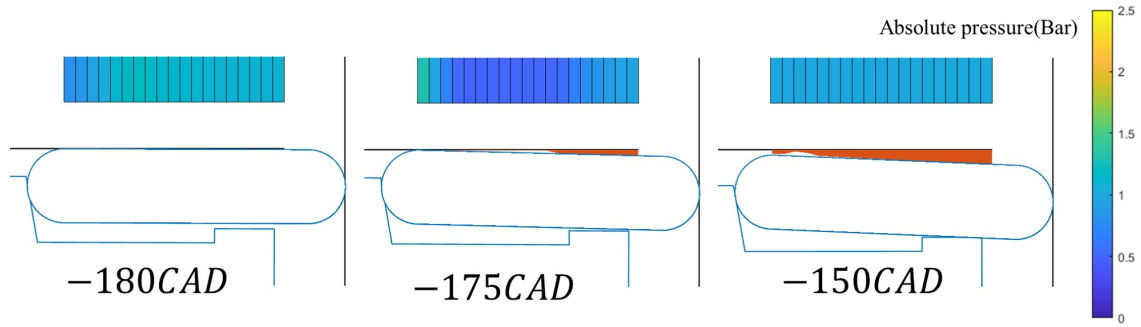Figure 4-5: Pumping Details when Rail approaches Flank

Figure 4-6: Pumping Details when Rail leaves Flank

roughness level and mostly occupied by oil film thickness. When the rail has the tendency to lift and increase the volume of the liquid, as a response the liquid will generate a negative pressure in the middle and suck the liquid from two boundaries. In reality, the dissolved gas vaporizes at rapid pressure drop. In the numerical implementation, there is a lower limit of pressure in the pumping zone, as cavitation pressure. In this figure, at $-175°$CA the pressure drops to negative in the middle along with an air bubble, gas occupies larger volume at low pressure. This negative pressure can hold the rail back to flank and prevent it from further lift for a while. Eventually at $-150°$CA clearance opens and air flows in from ID boundary and recovers the pressure loss.

As stated earlier, the oil flow in/out of the clearance is also one of the main focuses of this work. Figure 4-7 shows the accumulated oil flow through the four boundaries counting from the intake TDC and the convention for positive direction. In this thesis, all the air/oil flow released from upper regions of piston to lower regions is denoted as positive. Specifically, in the oil control ring groove, oil flows from 3rd land to groove,
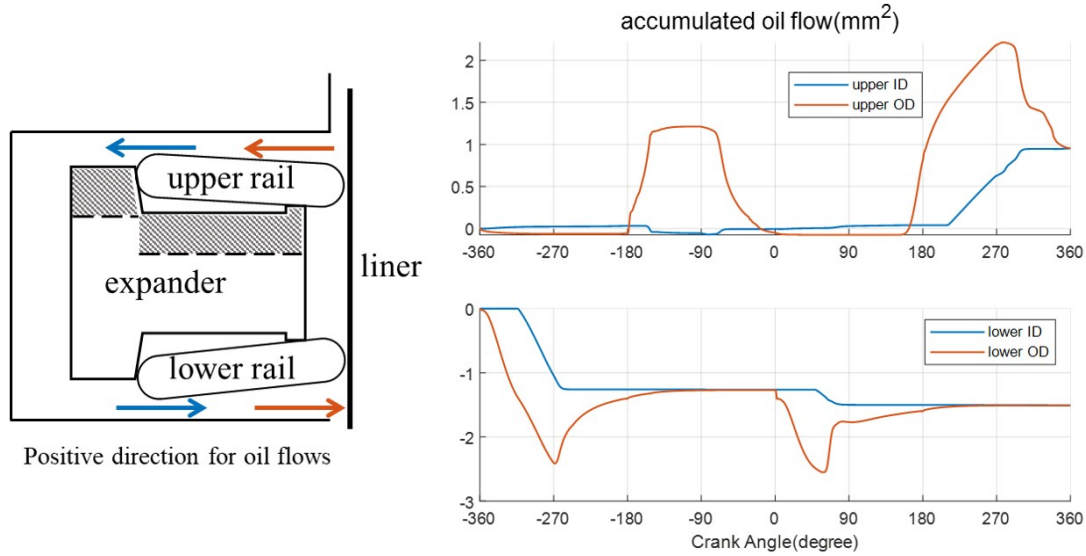
Figure 4-7: Oil Flow through Flank Clearance

from groove to 4th land have the positive sign. For the upper clearance, there are two peaks of OD oil flow after two BDCs ($-180°$CA and $180°$CA), corresponding to the upper rail lift by inertia force. While only the later one does penetrate through the pumping area to ID, this is because it takes time for oil to transport to the other side. There will be no net flow if the clearance closed before the oil reaches ID, all OD oil will be squeezed back as the first OD oil peak shows. In order to get net oil flow, there are three essential requisites: open clearance, pressure difference and oil supply on the boundary.

Rail liner lubrication

Other than pumping, rail liner lubrication is another possible passage for oil leakage. There are two supplies for inlet oil at the rail lubrication interface: liner oil and bridging. Figure 4-8 shows the scraping process for two rails. In the down stroke, the fully lubricated skirt area will leave oil on the liner with oil film thickness h1, two rails will scrape most of the oil and remaining oil film thickness is h_2 at sub surface roughness level. In the up stroke, if the upper rail cannot fully bypass the oil film thickness h_2 and assuming the trailing oil thickness is h_3, then $h_2 - h_3$ is the up-scraping amount into the 3rd land.
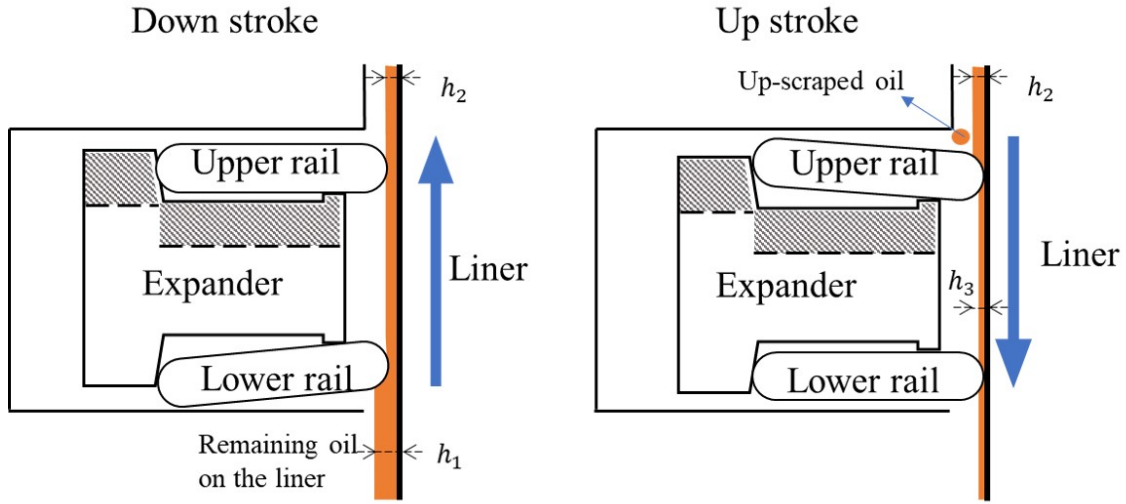
51

Figure 4-8: Rail Scraping Mechanism

Bridging specifically refers to a phenomenon of oil transport from piston to liner. Fang[6] studied the high-speed bridging in piston land and between two lands of twin-land oil control ring. Bridging may also happen between TPOCR rails. Figure 4-9 shows the mechanism for TPOCR bridging around BDC. When oil from the top of oil control ring groove is dragged down by inertia, due to the hollow design of the expander, it may fall on the expander or lower rail depending on local pitches and then attach the liner and eventually hit the upper rail profile.
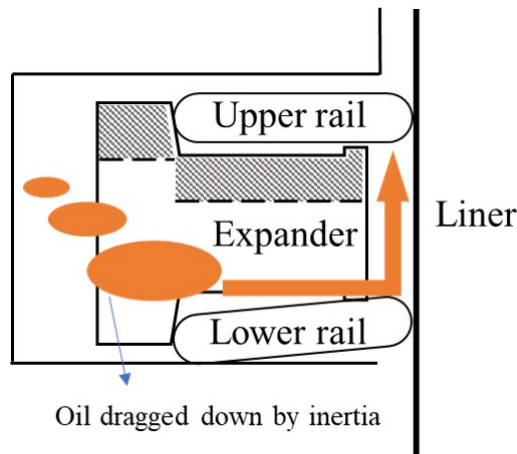

Figure 4-9: TPOCR Bridging Mechanism

Bridging adds additional oil on the liner to supply the upper rail and effectively

nullifies the oil control of the lower rail. Thus more oil may pass the upper rail, increasing possibility of net oil transport to upper regions, through, for instance, up-scraping in the ensuing up-stroke by the upper rail. One of the main effects oil accumulation inside the oil control ring groove may lie on it affects the timing of oil bridging and thus oil supply to the upper rail during down-strokes. In the sample results, the bridging timing is also an input. Figure 4-10 shows the minimum clearance between upper and lower rail and liner. The hydrodynamic pressure is proportional to velocity so the rails see a larger clearance in the middle stroke. The two spikes after TDC corresponds to the bridging input. If the rail is fed with flooded boundary conditions, the clearance tends to increase.
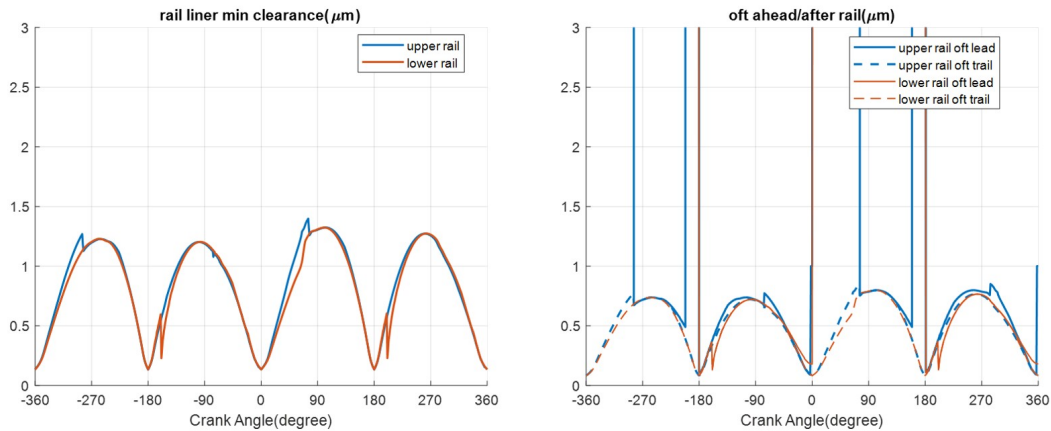

Figure 4-10: Rail Liner Minimum Clearance and Liner Oil Thickness before/after Rail

Figure 4-10 shows the oil film thickness ahead and after the rail pass within one engine cycle, note the plateau above $3\mu m$ is assumed to be flooded due to bridging or lower rail down scraping. Notice the integral area between the blue solid line (upper rail lead) and dashed line (upper rail trail) in exhaust/compression stroke, it indicates the amount of up scraped oil into the 3rd land.

4.3 Effects of engine load/speed on rail motion

There are two ways engine load may affect rail motions. First is direct pressure force on upper rail. Higher engine load corresponds to higher cylinder pressure and

generally also indicates a higher 3rd land pressure. In a typical modern gasoline engine, 3rd land clearance is on the order of a few hundred micrometers and TPOCR upper rail is directly exposed to this clearance. Additionally, there are two edges in the rail face exposed to gas pressure besides the profile where sustains the asperity contact or lubrication. Through the upper edge 3rd land pressure provides extra rail force to balance to rail tension. The 3rd land pressure variation is much smaller than the lubrication pressure so its influence on lubrication is neglected here. Secondly, engine load will change the pumping behavior. Higher 3rd land pressure may penetrate through the pumping region and additional pumping pressure alters the rail dynamics. From 2DLIF experiments, higher engine loads usually see less oil accumulation in 3rd land and presumably oil boundary condition will be changed. In this part, the oil boundary condition is fixed since the relationship between load 3rd land oil amount is not explicit.
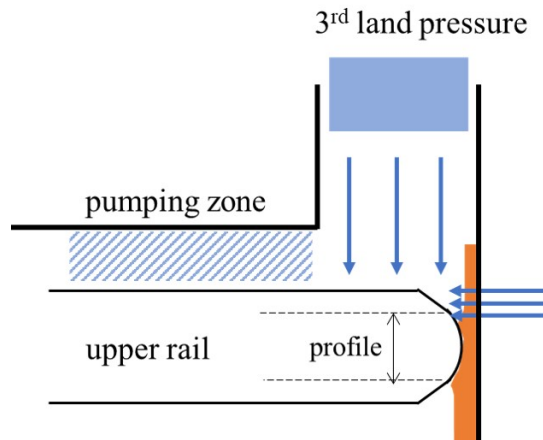

Figure 4-11: 3rd Land Pressure Effect on Upper Rail

Figure 4-12 shows the rail motions of three cases: 5000rpm/700mBar, 5000rpm/500mBar and 5000rpm/300mBar. For intake and compression stroke, the rail motions are similar considering 3rd land pressure variation is small compared with combustion process. In the expansion stroke, upper rail lifts at different timings. In the 700mBar case, the upper rail lifts before 90°CA and 300mBar cases lifts before 180°CA. For the lower rail, the clearance closes earlier at higher load in expansion stroke corresponding to the early lift of upper rail.
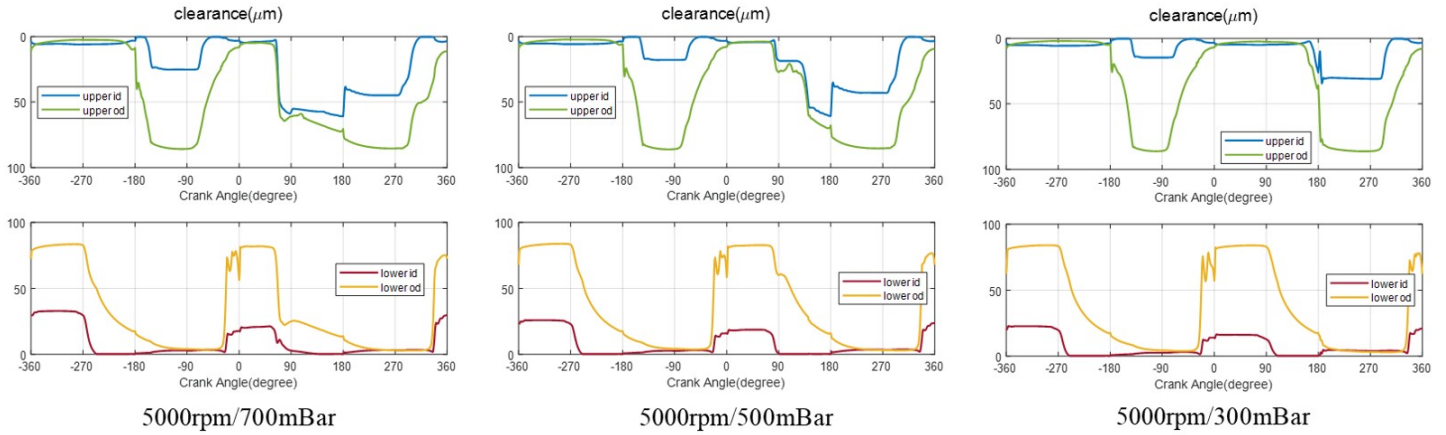
Figure 4-12: 5000rpm Load Effect to Rail Motions

Figure 4-13 shows the rail motions at 3000rpm, with 700/500/300mBar intake pressure. Compared with 5000rpm, the magnitude of inertia reduces by 64% at 3000rpm. With 300mBar intake pressure, the upper rail clearance is close to zero meaning the pumping suction force can hold the rail throughout the entire cycle against the combination of inertia, friction and 3rd land pressure. In 700mBar case, even the upper rail can be lifted by 3rd land pressure, the downward inertia is not enough to balance the friction and maintain the clearance in expansion stroke, so the upper flank clearance closes at 90°CA earlier than the 5000rpm case.
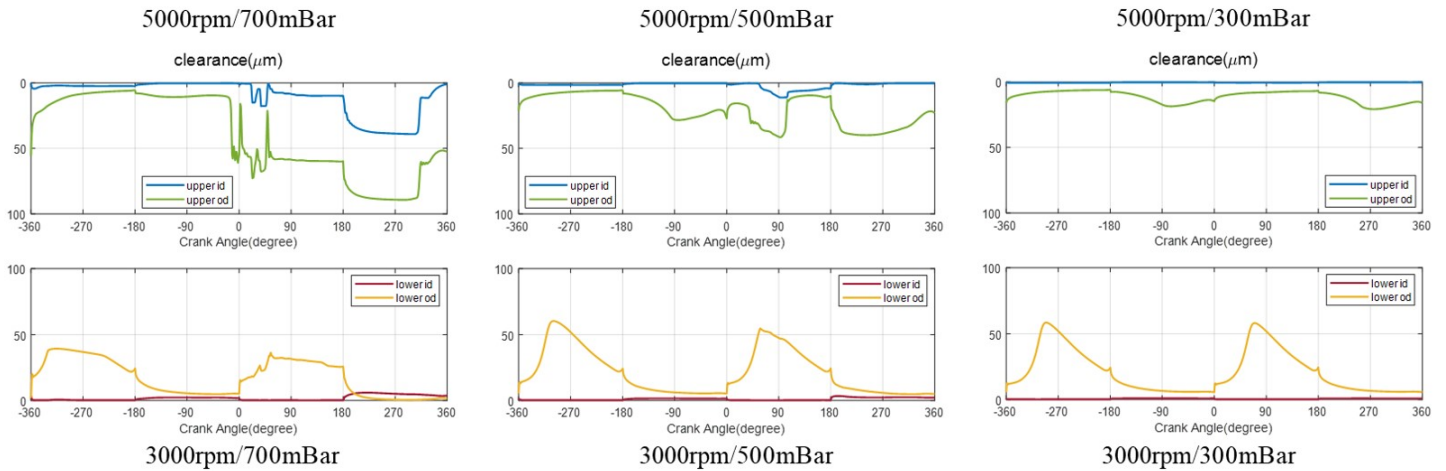

Figure 4-13: 3000rpm Load Effect to Rail Motions

The load effect mainly changes rail behavior in expansion stroke by opening up the

clearance. Ideally, the additional 3rd land pressure helps release oil accumulation by flushing oil into the pumping zone, while this depends on the oil amount and motions in 3rd land.

Engine speed is another important working condition affecting rail clearance. Inertia is proportional to square power of speed, at high speed more lift is expected for the rail. As shown in figure 4-14 , in both 4000rpm and 3000 rpm case, there is barely any lift for upper rail in the intake compression stroke. While in 5000rpm case, both upper rail ID and OD are lifted. This lift can be dangerous for oil leakage from groove ID. In the intake stroke, the 3rd land pressure can be below atmosphere in gasoline engines, it is possible to suck the oil to 3rd land if there remains oil in the groove ID boundary.
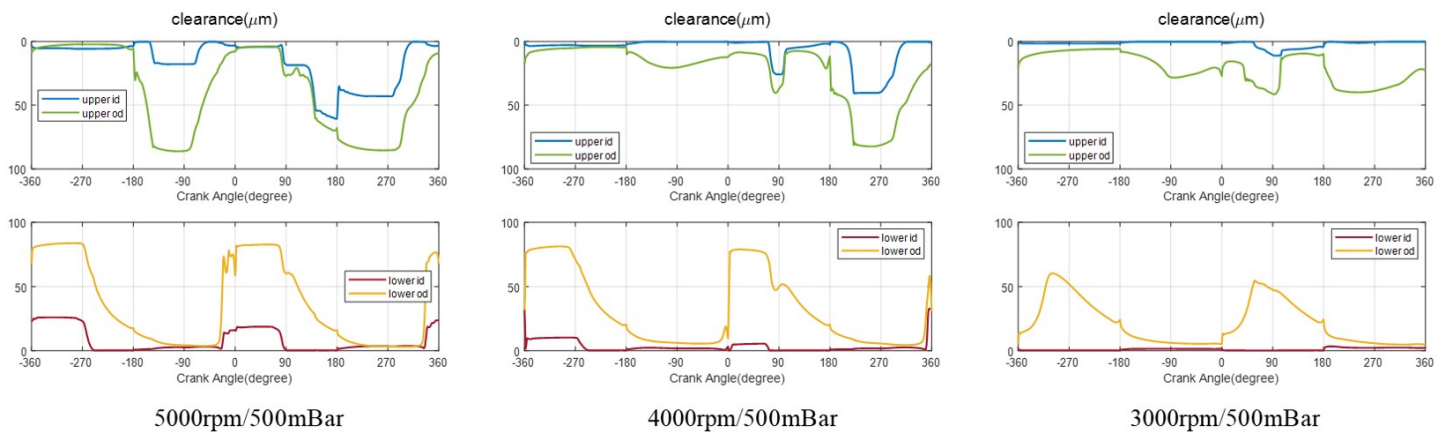

Figure 4-14: 500mBar Speed Effect to Rail Motions

The trend of lower rail motion is similar to the upper rail, higher speed allows more inertia to dominate other forces and opens the lower flanks clearance. The oil supply from lower rail OD is more less independent of ring pack system. Fang[6] developed a correlation for the skirt oil supply at lower rail OD in piston down stroke, the dynamic pressure also goes up with engine speed. Both clearance and boundary pressure favor high speed working conditions, this means the total oil enters the ring pack system is greater at high load.

Chapter 5

Comparison with 2DLIF experiments and further discussion on TPOCR oil transport

5.1 Introduction

Experiments and simulations are a duality of tools in the development of industrial engineering system. In most of the experiments, not all the data are observable so simulation can help explain the phenomenon. On the other hand, people don't trust simulation so more convincing experimental data is used to validate the models. This is not always the case, especially when we are still in the process of exploring and learning the mechanism and optimization direction for a physical system such as the three-piece oil control ring (TPOCR) lubrication. From another perspective, measurement or sampling may also have error and simulation is always consistent to the physical understanding as long as the algorithm is correct.

In terms of upstanding the ring pack performance, the first level is the structure. With a static finite element analysis, the ring conformability to the liner can be well predicted. The second level is gas flow. Considering the gas flow is mostly laminar and occupies the majority of the ring pack spare space especially around the top two

rings, we can also predict bulk gas flow with high confidence by coupling the gas flow with the ring dynamics and neglecting the oil. The structure and gas flow can be validated in some ways such as the tension measure apparatus and pressure sensor, while the oil transport does not have this advantage thus its mechanism remains unclear for people especially around oil control ring zone. Because oil only occupies a small volume compared with gas and it always shakes up and down by inertia in the reciprocal piston, it is difficult to capture oil behavior from experiments. From the modeling perspective, although it is all governed by the Navier-Stokes equation, there exist various scales of oil transport so traditional CFD method may not work in the connections between the rail liner lubrication and piston land oil movement.

With limitations of both sides, the relationship of experiments and simulation becomes more less mutual improvement and they share equal contribution in the research process in our lab. During the process, the 2DLIF videos may inspires additional understanding of physics into model development, and in turn, models may predict interesting behaviors and solidify the experiments. In this chapter, the 2DLIF experiments from Ahling[8] will be used to compare with simulation results. The goal of introducing the 2DLIF experiments is not only validating the model, but to illustrate the TPOCR behavior and oil movement together the TPOCR model.

5.2   2DLIF experiment setup

Figure 5-1 shows the setup of 2DLIF experiments by Ahling. Through a sapphire window on the cylinder liner, 8 cameras location captures the whole engine stroke along the axial direction.

Figure 5-2 is a sample image from 2DLIF experiment during early exhaust stroke. On the left is the full image from camera, brightness of the picture means the intensity of oil fluorescence. A further magnified view of TPCOR is on the right showing the details of TPOCR. For each rail, there exists a grey-black-grey stripe corresponding to the upper edge, contact profile and lower edge of the rail face. In early exhaust stroke, the upper groove clearance is open so we can see an additional black line above
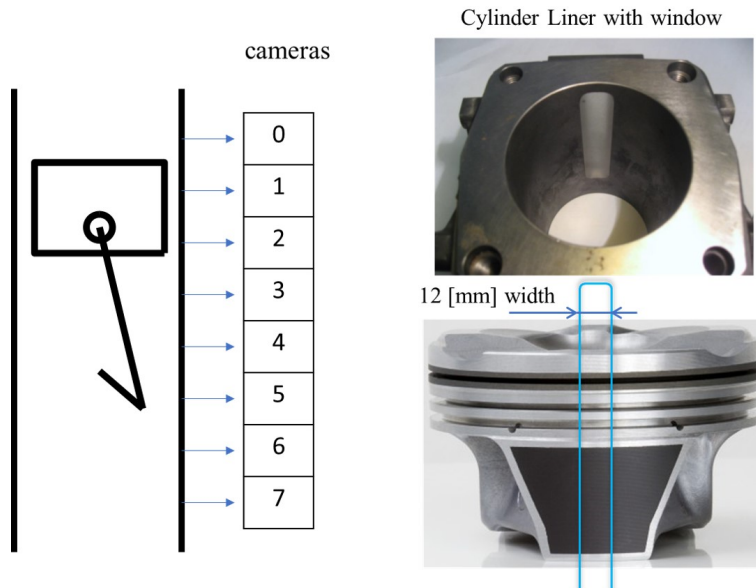
58

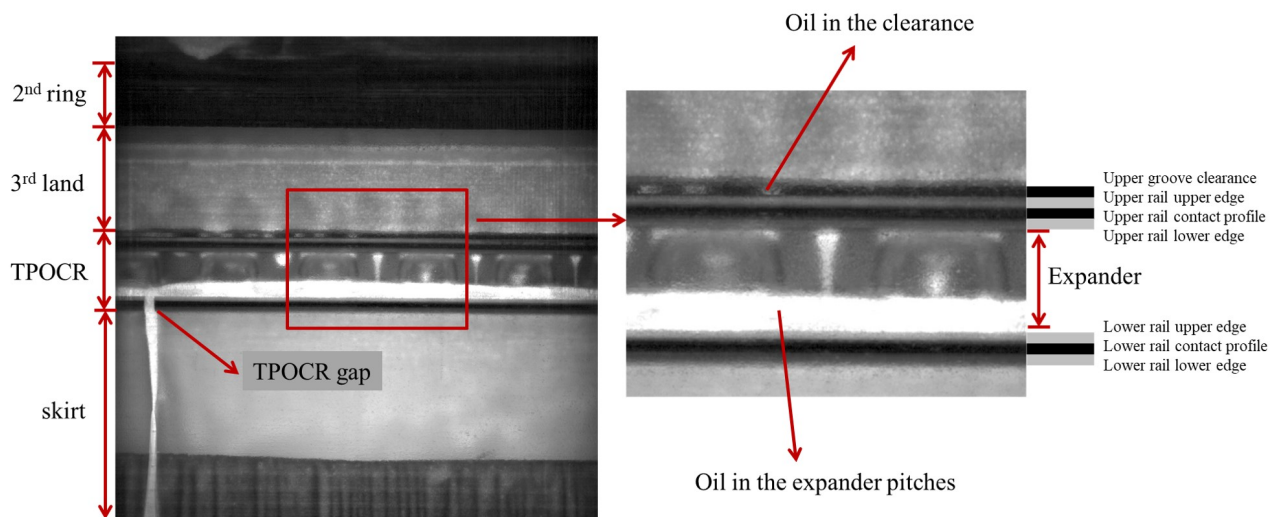Figure 5-1: 2DLIF Experiment Setup

Figure 5-2: 2DLIF Image Example

the upper rail.

Because the piston is moving at high speed and camera is static, it is difficult to quantitatively extract the rail motions from snapshots. Instead, for the following comparisons, we will choose 2 pictures at similar liner location but from different strokes, align them with certain reference in the exact same lateral position. With this approach, it is possible to tell the relative displacement of rail motion and show the accordance with simulation results.

5.3 Comparison between 2DLIF experiment and simulation results

In this section, the engine is running at 3000rpm/700mBar working condition. Figure 5-3 shows the simulated rail groove clearances from TPOCR model. A few crank angles are chosen for comparison with 2DLIF experiments and their timing is marked with grey lines.
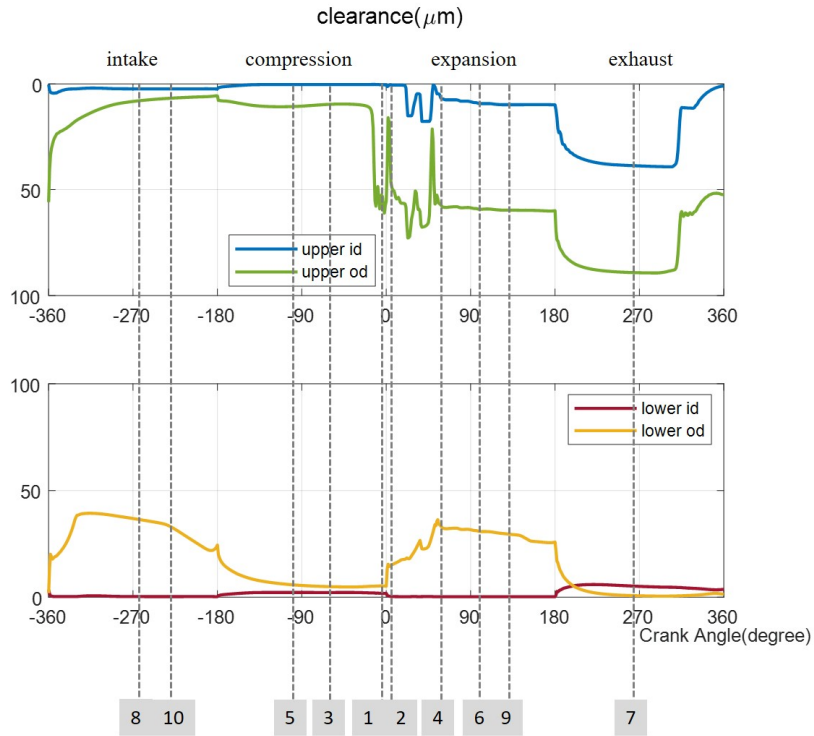

Figure 5-3: Simulated Rail Motions and Selected Moments for Comparison

Around combustion TDC

Figure 5-4 shows the simulated TPOCR behavior around combustion TDC plotted into a graphical cross section. Moment 1 and 2 indicates the 3°CA before top dead center (BTDC) in compression stroke and after top dead center (ATDC) in expansion stroke. Before TDC, rail friction is downwards in up stroke and together with 3rd land pressure, the upper rail clearance opens. Right after the TDC, the friction shifts direction so the rail is pulled back to flank.
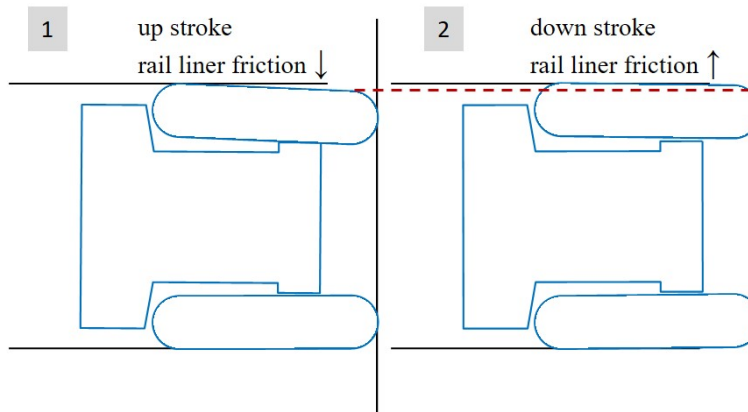

Figure 5-4: Simulated TPOCR Motion Moment 1,2

Figure 5-5 shows the 2DLIF pictures of TPOCR motion at same crank angles, left half is cropped from compression stroke and right half is from expansion. We align the axial location of 2 pictures with the skirt features in the same lateral position as reference. In the expansion stroke, clearly the upper rail is higher than the compression case, which is consistent to the simulation prediction. In the beginning of expansion stroke, there exists a bright line of oil left by the upper rail. Presumably this oil line contributes to the oil supply to the 3rd land from TPOCR. The upper rail squeezing and up-scraping are two major sources for oil line, while it is difficult to tell which one is more important.

crop

compression
(~3CAD BTDC)   1 | expansion
                        (~3CAD ATDC)   2

oil

alignment
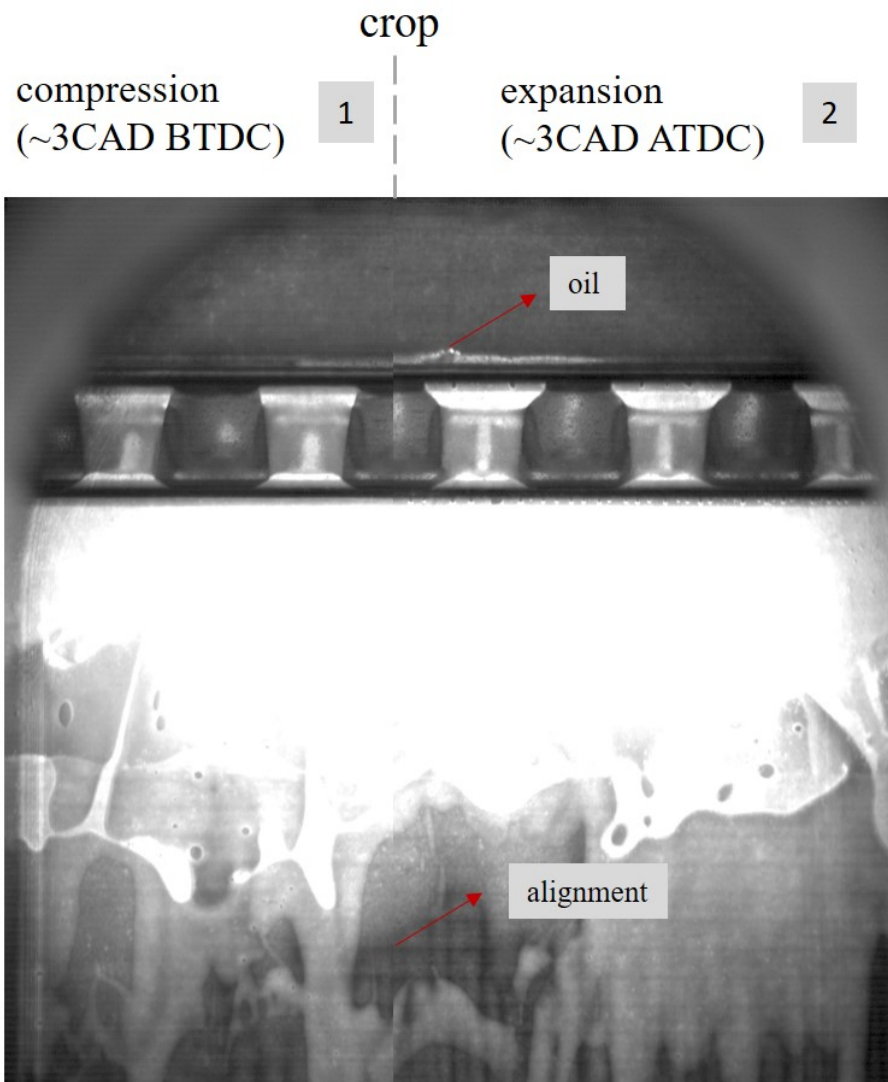
Figure 5-5: 2DLIF Image Comparion Moment 1,2

expansion
(~12CAD ATDC)

Oil left
on the liner
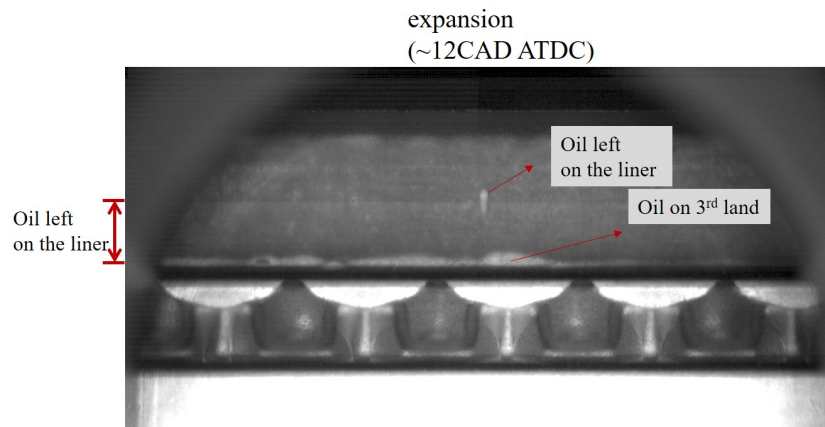
Oil on 3rd land

Oil left
on the liner

Figure 5-6: Oil left in the 3rd Land after Intake TDC

Figure 5-6 shows the evolution of this oil line at 12°CA ATDC, some of the oil attaches liner so leaves a thicker oil layer on the windows, other stays in the 3rd land/upper rail corner held by surface tension.

In this setup, the oil boundary condition for pumping model is shown is fig5-7, 0 means dry boundary and 1 means the boundary is fully flooded with oil. The upper OD and ID boundary conditions are correlations from Fang, the ID boundary conditions come from the MOR method in chapter 3. Inertia is the major driven force for land and groove oil movement and piston velocity direction dominates the skirt oil supply at lower OD. The boundary conditions used here are ideal cases neglecting the rail dynamics and rail liner interface oil. When the inertia is pointing upward, the surface tension can hold some oil at lower 3rd land. In the exhaust stroke, the up-scraping oil above the upper rail may also flow inward and fill the groove clearance, this explains the oil source for upper rail squeezing right after TDC. These are all important factors worth investigation in the future.
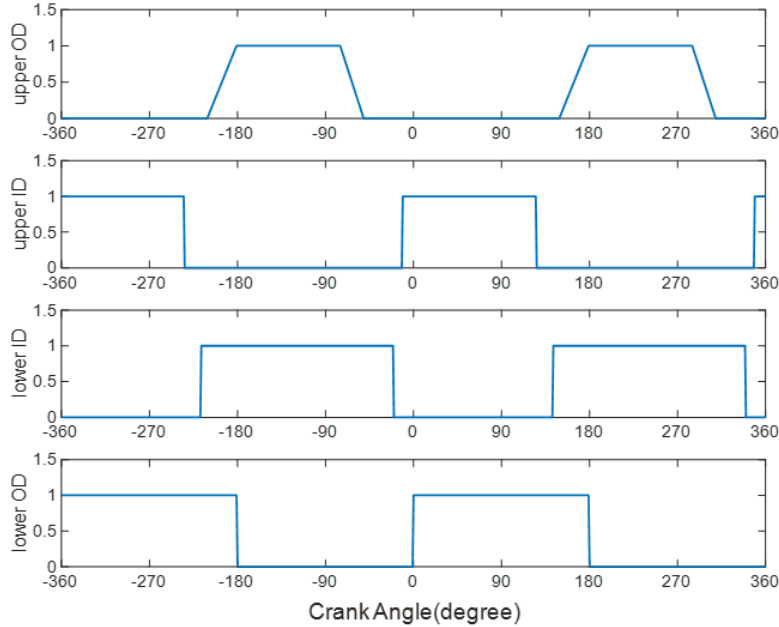

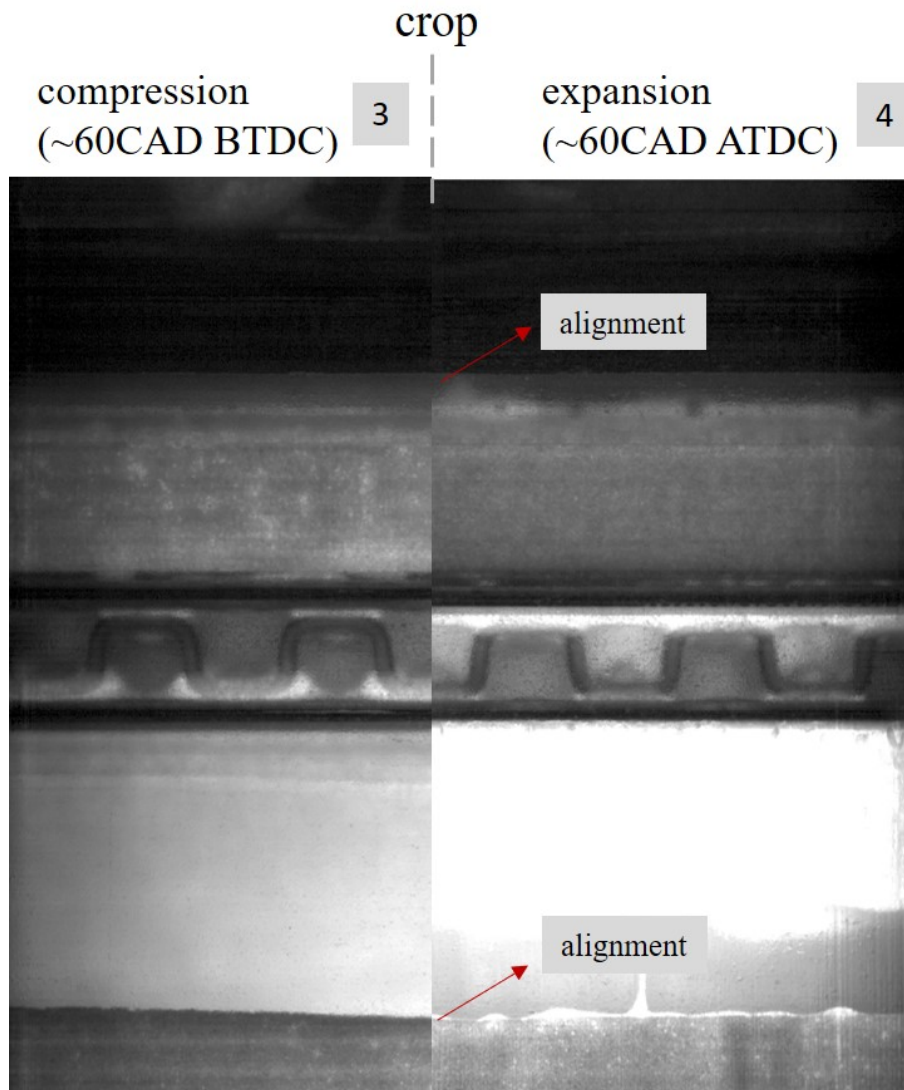Figure 5-7: Boundary Condition Input for Simulation

Figure 5-8: 2DLIF Image Comparion Moment 3,4

If we compare the rail motions further away from TDC, as shown in figure 5-8, the relative position of upper rail shifted at $60°$CA before TDC and BDC. In this cropped picture we align the 2nd ring and skirt for vertical location. This result also matches the simulation prediction. Notice that the upper rail relative vertical position in intake and expansion stroke shifted. In the expansion stroke, the upper rail is pushed down by 3rd land pressure. The whole process of relative position change of upper rail from $-60°$CA to $60°$CA can be explained in the following diagram in figure 5-9.
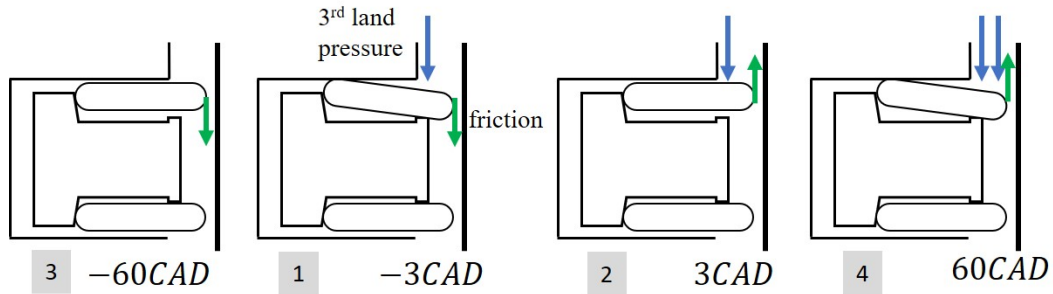
Figure 5-9: Mechanism for Upper Rail Motion around Combustion TDC

Starting from phase 3, piston is moving up but the downwards rail liner friction is not able to overcome the inertia and pumping force so rail stays at the top. In phase 1, 3rd land pressure begins to increase and lifts upper rail together with the friction. Later friction shifts direction after TDC and rail is dragged back to flank. 3rd land pressure will further increase due to combustion and blocked groove passage, it beats the friction and inertia force to push the rail downwards again. In the simulation clearance fig5-3, the upper OD position is fluctuating after the TDC, this is also from block-release balance of 3rd land pressure.

Compression/exhaust mid stroke
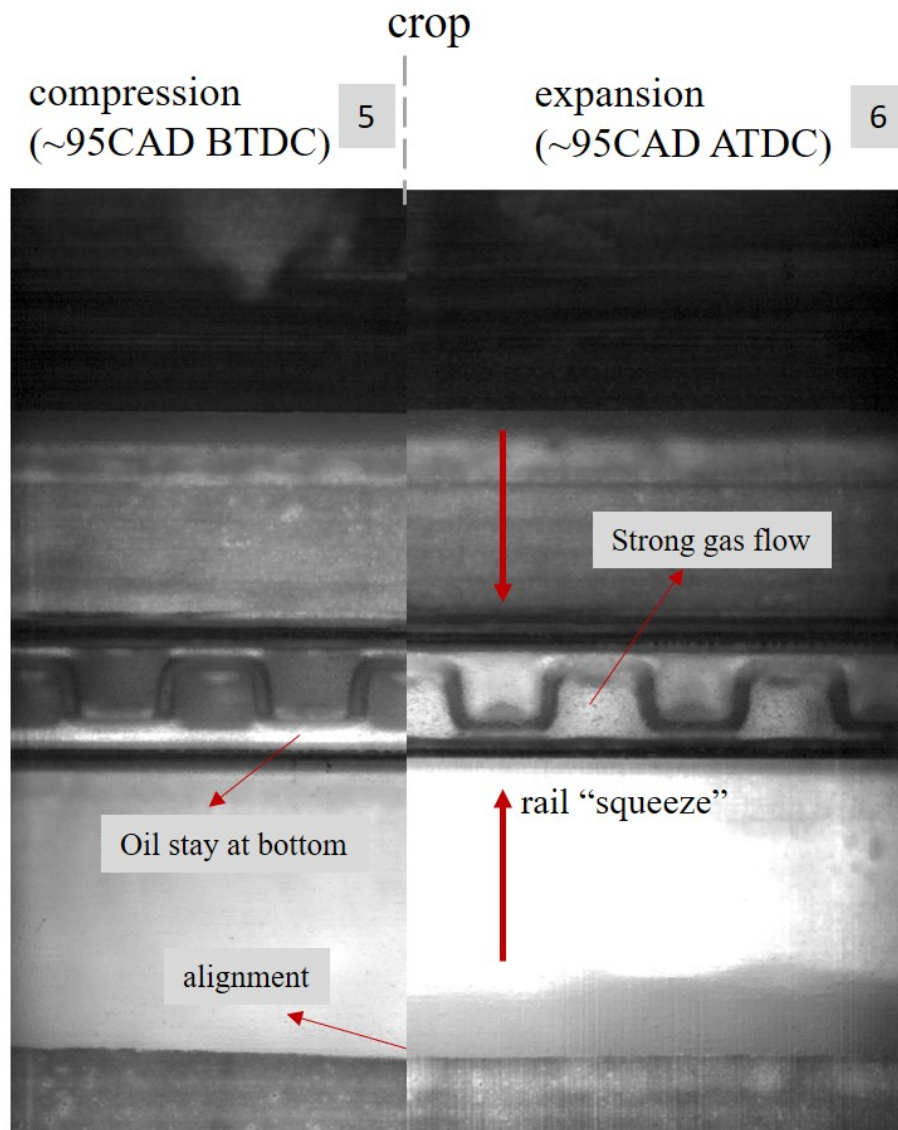
Figure 5-10: 2DLIF Image Comparion Moment 5,6

Figure 5-10 shows the 2DLIF results in compression/exhaust mid stroke around 95°CA BTDC/ATDC. In this part we align the skirt feature. A clear observation from the expansion stroke is that both upper and lower rail clearance are open, so the rail is "squeezed" from the image compared with compression stroke. The simulated relative position in figure 5-11 shows the same result. When the 3rd land pressure grows in expansion stroke, upper rail will be further pushed down. For lower rail, the

Figure 5-11: Simulated TPOCR Motion Moment 5,6

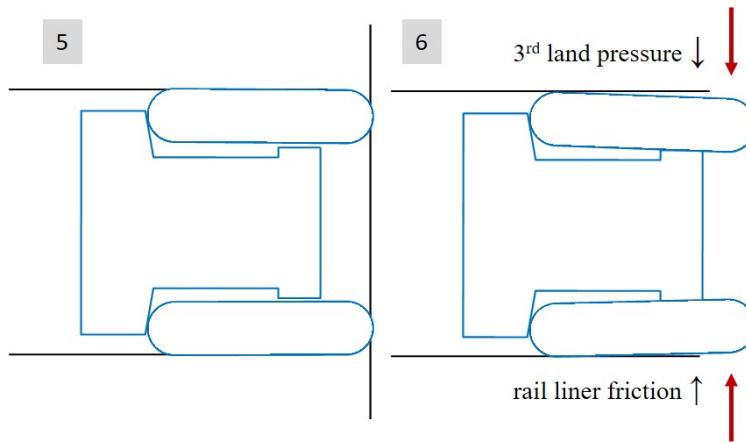pressure effect is less important and inertia force is relatively small around mid-stroke, so the OD clearance is dominated by rail liner friction.

The interesting thing in this snapshot is that a strong gas flow inside the groove is observed during expansion stroke. These gas flows come from the 3rd land gas releasing through upper rail groove and may trigger strong bridging effect to upper rail interface.

In the compression stroke, there is oil accumulation above the lower rail driven by inertia force. This oil can move freely between the expander pitches and inside the groove, and can potentially become the supply source for upper rail groove leakage and up scraping.

Exhaust/intake mid stroke
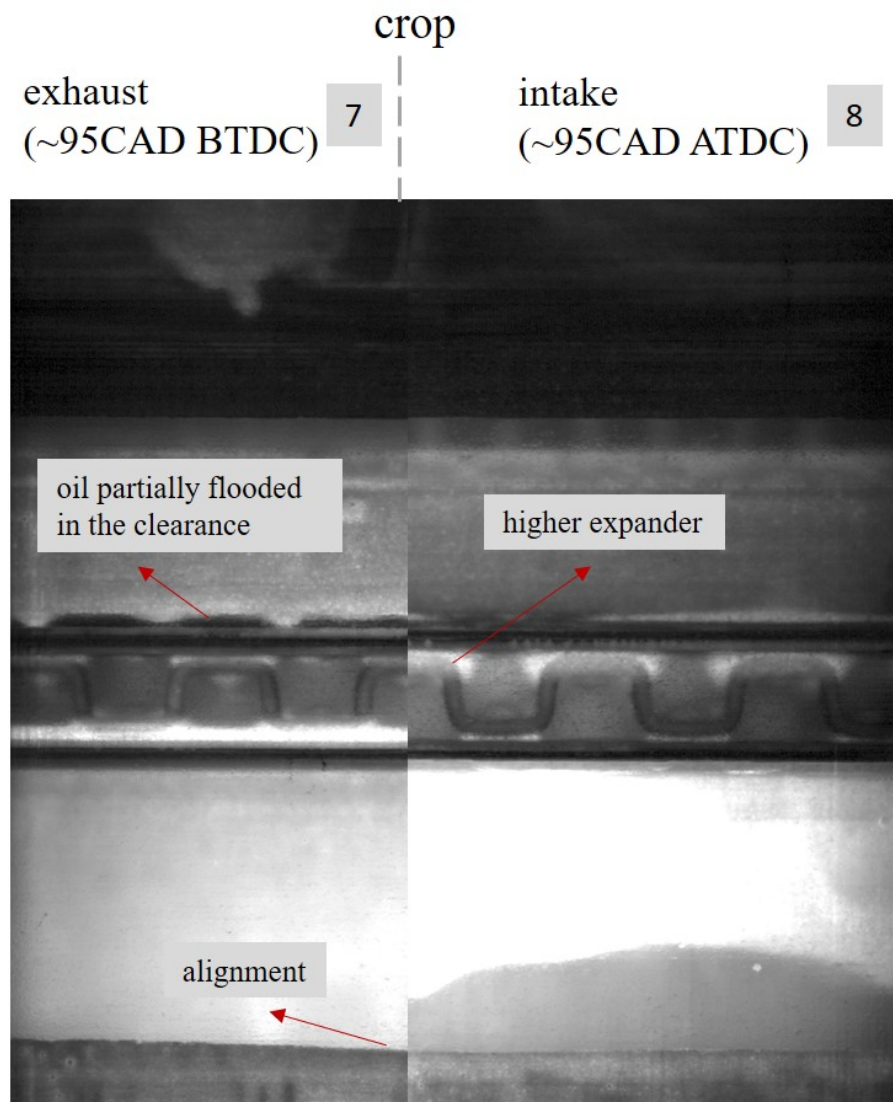
Figure 5-12: 2DLIF Image Comparion Moment 7,8

During the intake and exhaust mid-stroke, inertia is small and the 3rd land pressure is much lower than expansion stroke so the TPOCR axial motion is dependent on the rail liner friction. In the exhaust stroke, piston is moving upwards so friction drags both rails downwards. In the intake stroke, the upper rail stays at the top and lower rail will be twisted positively by friction. Through the asperity contact between rails and expander step, the expander motion would also follow the friction direction. As shown in figure 5-12 and figure 5-13, both simulation and experiments identify a

higher expander in intake than exhaust stroke.
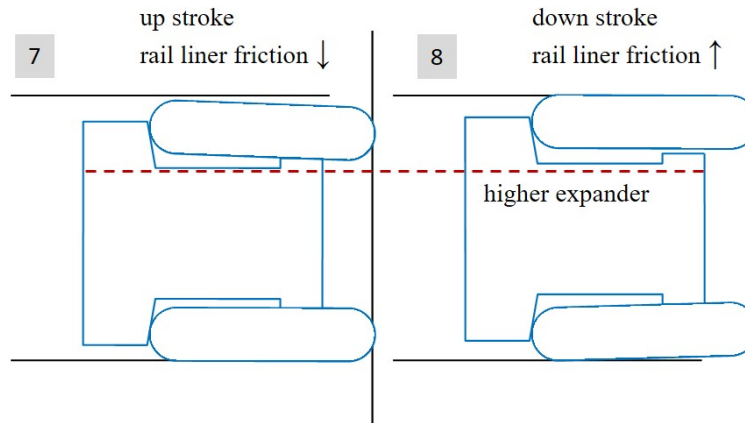
Figure 5-13: Simulated TPOCR Motion Moment 7,8

In the 2DLIF video, the upper rail clearance is open during the exhaust stroke and oil boundary is never full. For example, in this image, the oil is mostly on the boundary. This does not necessarily indicate the oil boundary condition for exhaust upper rail OD should be treated always dry in the model. It is possible the 3rd land oil flow is flushed into the groove by pressure or inertia as long as it arrives so the inlet so the inlet is clean. Besides, the up-scraped oil may also flow into the clearance. Once the oil gets in, it may be released into ID or squeezed back to 3rd land after intake TDC.

Around expansion/intake BDC
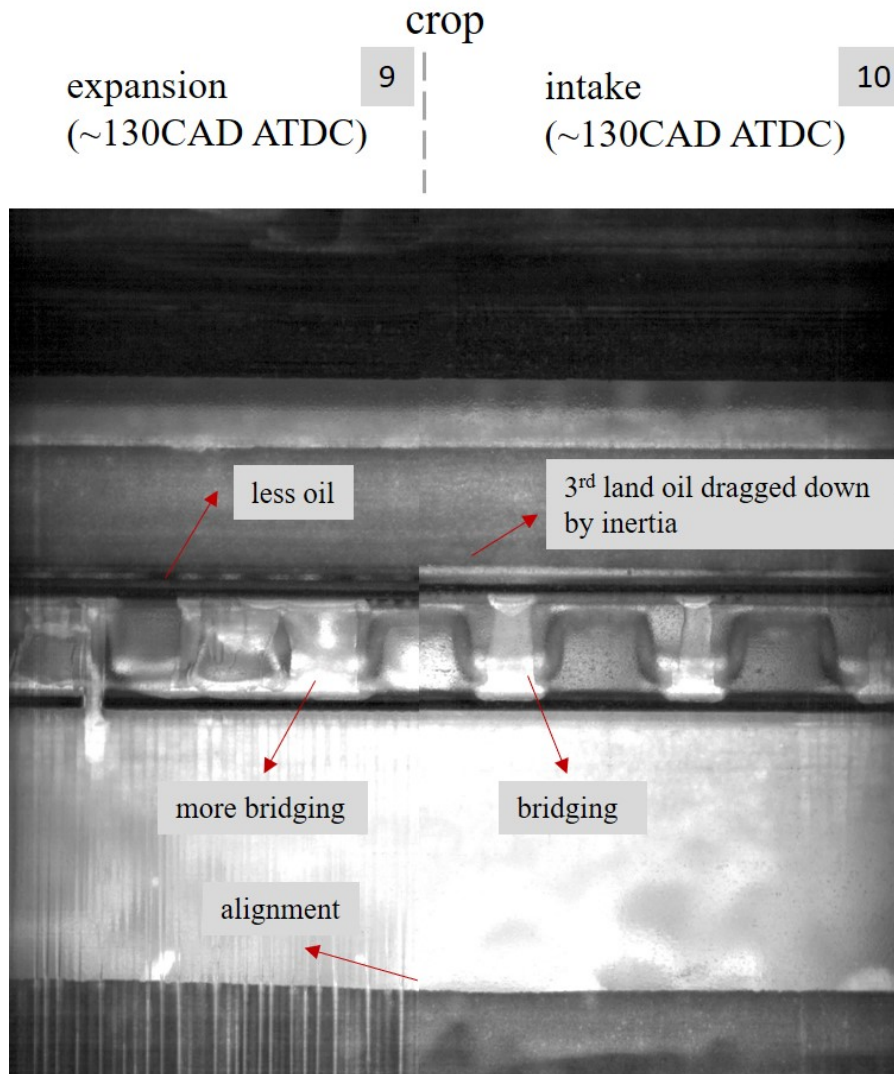
Figure 5-14: 2DLIF Image Comparion Moment 9,10

Figure 5-14 is the comparison of two down strokes: expansion and exhaust. The purpose of this comparison is mainly for the oil status. When piston approaches BDC in downstroke, the oil inside the groove will be shaken down and bridge to liner. The moving liner drags the bridging oil to the upper rail and supplies the upper rail. In this snapshot, bridging occurs in both stroke but more dramatically in expansion stroke. The major reason here is the strong gas flow from 3rd land pressure release as discussed. The other interesting point here is the oil distribution above upper

rail. Inertia is pointing downwards around BDC, intake stroke oil from 3rd land accumulates above the rail due to clearance closure. While in the expansion stroke, although there is less oil at the clearance. It is possible the 3rd land pressure flushes the oil into the upper rail clearance, only remaining oil is observable.

5.4 Summary

In this chapter, the rail motions and oil movement are studied by comparing the 2DLIF experiments and TPOCR model simulations. Despite the high speed piston motion, qualitative rail motions can be extracted thanks to the high resolution of the 2DLIF images. The rail motions prediction by TPOCR model match experiments at all the critical moments within one engine cycle. The expander axial motion is also observed from both sources. The comparison proves the capability of the TPOCR model especially in resolving the ring dynamics. From the modeling side, it explains the intrinsic mechanisms for the real time TPOCR motions captured from cameras.

The oil motion in 2DLIF images is rather complex but the general pattern can be explained by physics understanding, although some details are vague such as the source for the oil line left on the liner after intake TDC. In the TPOCR model, upper scraping always exists but not the rail flank squeezing. The current treatment for he oil boundary conditions are relatively ideal and need further refinement in the future.

The purpose of this section is to build a learning bridge between experiments and simulation, not just validating the model with the experimental data. In reality, experiments and simulations are both data and modeling in this process. The oil fluorescence is captured through a high speed camera, the pixels in the image can be biased considering the laser intensity and high speed engine vibration. Besides, we are inferring a 3D structure through a 2D image, therefore information loss is certain. From the other perspective, the experiment is another forward modeling process converting the working condition inputs into the observable data. The advantage of simulation is that this converting process is almost surely deterministic and all the mechanism is fully exposed. While it requires more assumptions of the hidden knowl-

edge like the oil boundary conditions which may be a mystery for either side. After all, both experiment and models are not perfect and it is necessary to have them compensate each other.

Chapter 6

Further parametric study on oil transport around TPOCR

6.1 Introduction

In the chapter 4, the TPOCR model is applied on the 2DLIF engine and sample results demonstrate the outputs of the model. The mechanisms of typical pumping pressure/oil and lubrication oil transport are explained with the example. The effects of working condition such as speed and load on clearance results are also illustrated. Chapter 5 explains the 2DLIF rail motions through the simulation and discusses the observable oil distributions and potential indication on boundary condition treatment. In this chapter, further parametric study on oil transport will show the sensitivity of working conditions and key design parameters. Firstly, we will study the oil leakage through lower flank clearance against speed and design parameters. For upper flank oil leakage, although there remains unclear oil boundary condition for future research, preliminary results on overall trend and mechanisms will be explored. In the end, we will discuss the upper rail up scraping effect.

6.2   Effects of engine speed on lower flank oil leakage

Most of the lubrication oil supply into ring pack comes from the piston skirt clearance. In figure 6-1, oil in the skirt clearance will be dragged into the skirt chamfer by the liner in the down stroke and potentially generates a boundary pressure at the groove clearance entrance or pumping zone. Fang[6] studied this process and derives a correlation for this outer end pressure:

$$P_{end} = 12.2 \cdot \frac{\mu U_l}{h_l} \cdot \frac{1}{(1 + 1.2 \cdot \frac{\nu L}{U_l h_l^2})^2} \tag{6.1}$$

Where P_{end} denotes the pressure at the pumping zone OD (outer diameter) pressure, μ and ν are the dynamic and kinematic viscosity of oil. L is the distance between pumping zone OD to liner, h_l is the skirt liner clearance and U_l is the liner velocity.

This dynamics pressure at the OD helps oil pumping through the groove clearance and if the ID(inner diameter) clearance opens, the oil may pass this gate and fill the groove and potentially move to upper part of piston. As shown in figure 6-1, the ear angle design in the TPOCR expander pad will provide a vertical component to push the rail to seal the ID clearance. At higher engine speed, we are expecting a larger P_{end} due to the higher liner velocity. Besides, the lower rail motion is dominated by inertia so higher speed leads to larger flank clearance.
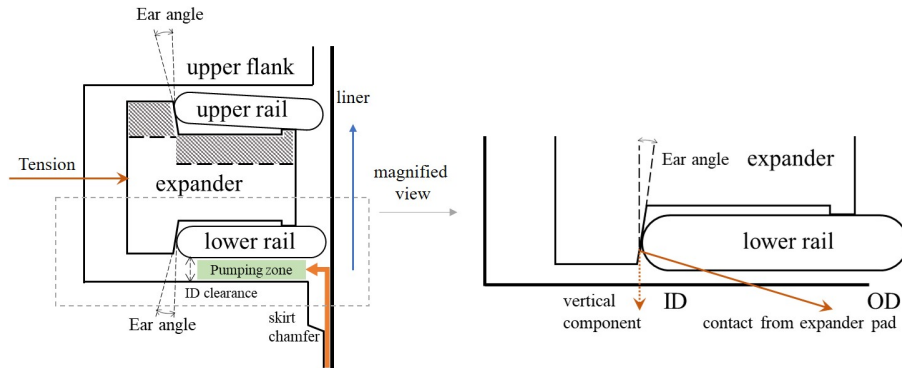

Figure 6-1: Configuration of Lower Rail and Skirt Oil Supply

Figure 6-2 shows the lower groove oil leakage at various engine speed from 3000-6000rpm and the ID clearance respectively. The negative oil volume means the oil

74

flows from lower rail OD to ID. The leakage flow rate and clearance grow with engine speed as expected. At 3000 rpm, the inertia is too small to lift the low rail ID clearance so oil flow is mostly blocked.
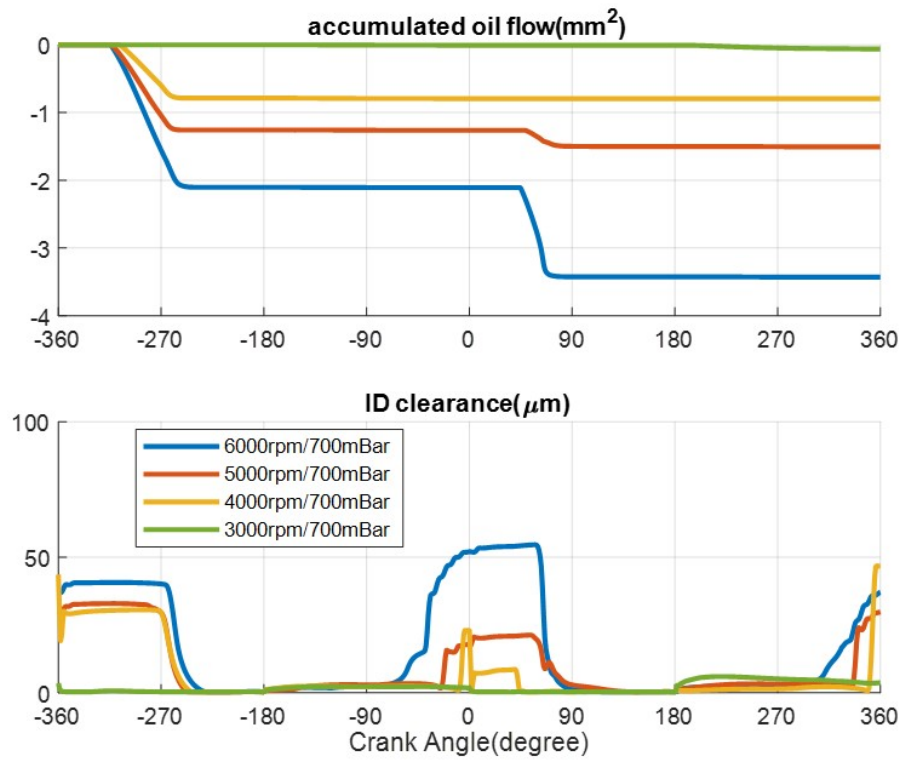

Figure 6-2: Accumulated Oil Flow and Clearance at Lower Rail ID at Different Speed

6.3 Effects of rail ear angle on lower rail groove oil transport at high speed

From figure 6-1, considering the vertical component is proportional to tan(ear angle), ideally with a larger ear angle a better sealing effect is expected, this intuition may not be true at high speed.
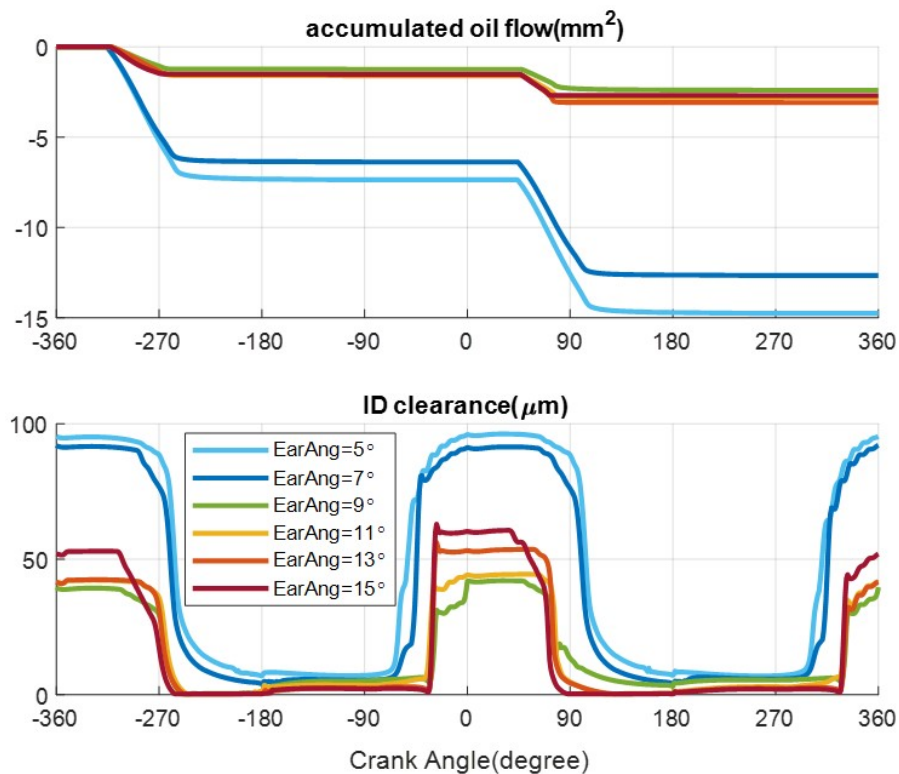

Figure 6-3: Accumulated Oil Flow and Clearance at Lower Rail ID with Different Ear Angles

Figure 6-3 shows the accumulated oil through the lower rail ID clearance counted from beginning of engine cycle and corresponding ID clearance for ear angle range from 5° to 15° and engine speed 6000rpm and default expander tension 21N. There is an optimal angle around 9° with lowest oil leakage and minimum overall clearance. The smaller ear angle results follow the intuition that small vertical component could not seal ID clearance well. Figure 6-4 explains the process why large ear angle may underperform.
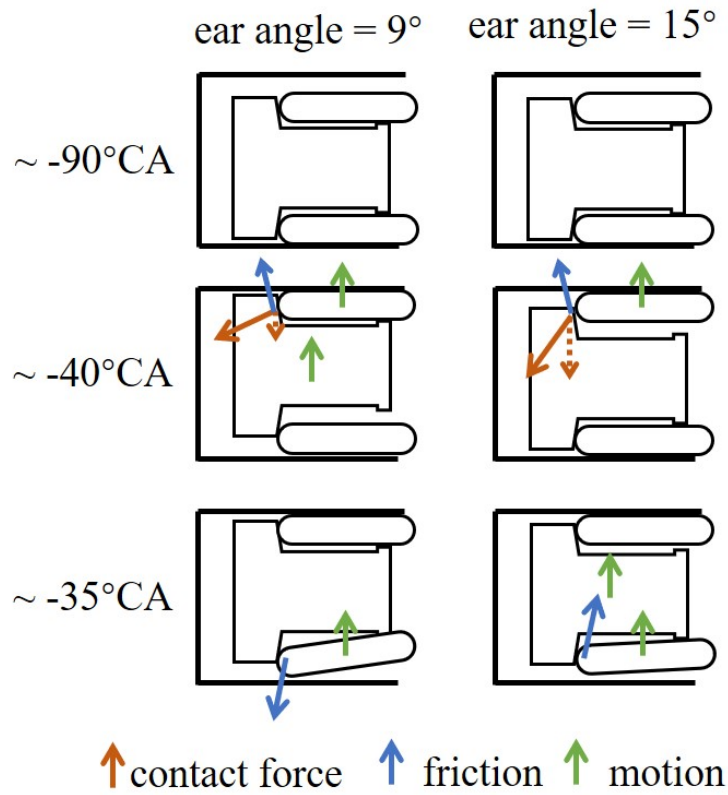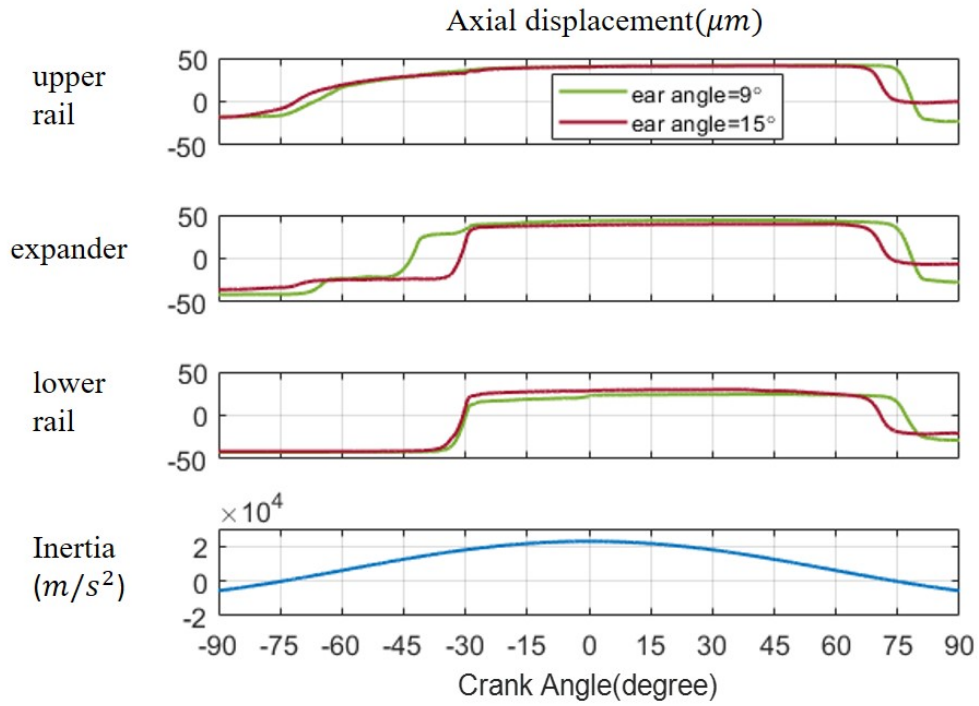
Figure 6-4: Mechanism for Lower Rail Oil Leakage with Large Ear Angle

The upper figure is the axial displacement of upper rail, expander, lower rail along with the inertia force around TDC area. Around $-90°$CA, both expander and lower rail stays at the bottom. After $-76°$CA, when inertia shifts direction, upper rail lifts first and then expander. Because in the upper pad we also have a larger vertical component in $15°$ case, the expander movement lifts a little bit then stopped. The $9°$ ear angle case can go all the way up. When lower rail starts to lift around $-35°$CA, in the $9°$ case because expander is already on the top, the pad friction is pushing the lower rail ID, but the $15°$ case expander is moving up with the rail, it's kind of dragging the rail when two parts are glued together by friction. The ultimate clearance in $15°$ case is greater than $9°$ which allows more oil to penetrate.

In the pad surface, there is a counterbalance between maximum friction and vertical component. With small ear angle, maximum friction always dominates the vertical component of contact force at upper pad thus expander can always be lifted with upper rail, so the lower rail clearance will decrease with more vertical component. After the ear angle passes the critical value, it is possible for expander to delay its lift timing with larger ear angle, later when the lower rail starts to lift, the expander is moving along with lower rail and even helping open the ID clearance. This explains the reason for optimal ear angle is $9° \approx \arctan(\mu_k)$, where μ_k is the friction coefficient we assume for the rail pad relative motion.

So far, we observed this phenomenon occurs on relatively high engine speed, at lower speed the inertia is able to lift the lower rail ID into a large clearance with a reasonable ear angle design.

6.4 Effects of expander tension on lower rail groove flank oil transport

Another important parameter for TPOCR is the expander tension, similar to the ear angle, intuitively larger tension can seal the lower ID clearance better. Different to ear angle design, although extra tension may seal the oil very well, it may generate additional rail liner friction and cut down engine efficiency. Besides, the engine cylinder wall will distort by a few hundred microns due to engine thermal condition so the actual rail tension in engine operations may deviates from the design value. From the industry experience, we are expecting a certain threshold for tension. When tension is below this value, the rail is not capable to seal the oil. When tension is above this value, the sealing performance reaches a plateau while extra tension is unnecessary. The optimal value for design tension should be above this threshold to guarantee the robustness under various working conditions such as large bore distortion.
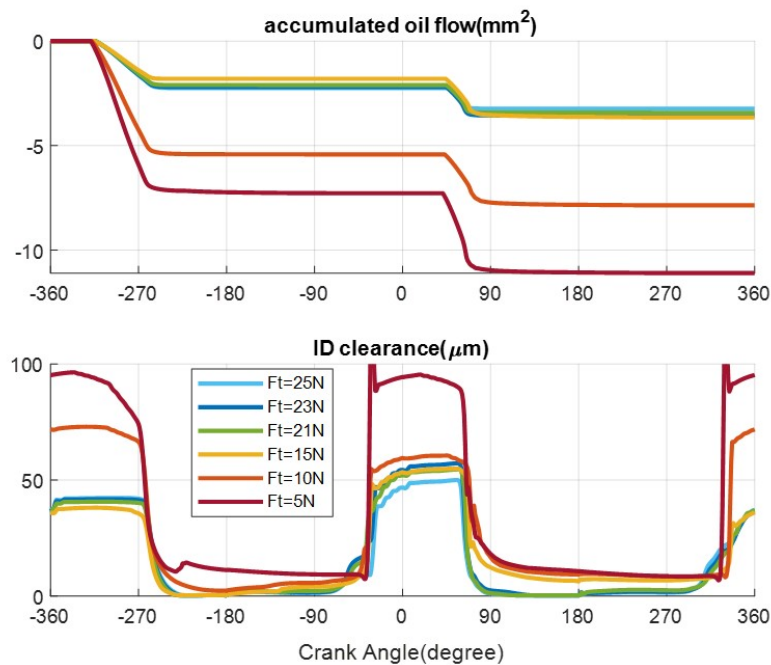

Figure 6-5: Accumulated Oil Flow and Clearance at Lower Rail ID with Different Tensions

In this part, 6000rpm is again selected as the vulnerable case for oil leakage with

higher inertia force and liner speed, the default expander ear angle is 10° from the 2DLIF experiment setup. Figure 6-5 shows the trend of lower rail oil leakage with tension ranging from 5N to 25N. In 5N case, the ID clearance almost reaches 100 microns around both TDCs, meaning under this tension the rail ID is not well controlled by expander ear angle so as the accumulated oil flow rate. The next step is 10N, ID clearance drops at combustion TDC with 3rd land pressure pushing all three pieces, but around intake TDC the ID clearance can still be opened up. After the tension reaches 15N, the clearance and oil leakages barely improve with increasing tension. In this simulation case, this threshold is around 15N.
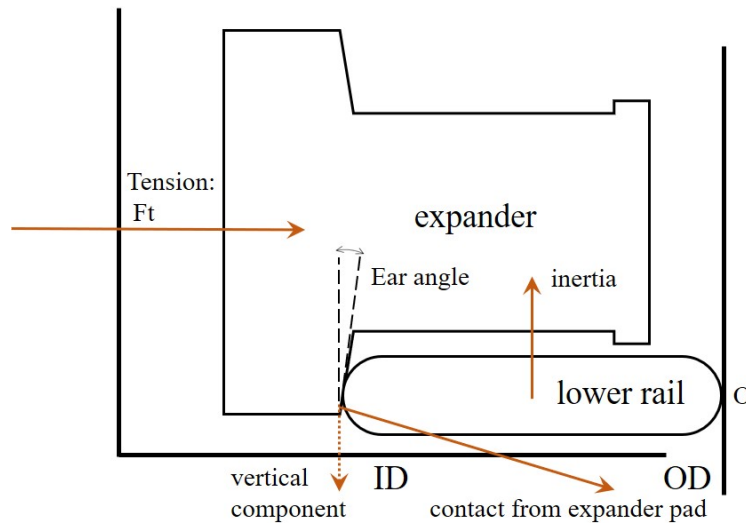

Figure 6-6: Configuration of Lower Rail

Although this threshold for rail tension highly depends on the real engine working condition and surrounding dynamic forces, we can roughly estimate this value by doing a simple calculation as shown in figure 6-6. Suppose we can neglect the forces to lower rail from groove flank, expander step, and expander pad friction, then build a moment balance for lower with rail liner contacting point O as fulcrum. The only contributing forces to torque are the vertical component and inertia force. Our rail weights around 2.5 grams and piston acceleration before ID opens up is around $7000 m/s^2$ so the inertia force is around 18N. Then with momentum equation:

$$Ft_c \cdot 2\pi \cdot \tan(\text{ear angle}) \cdot \text{rail width} = \text{inertia} \cdot m_{rail} \cdot \text{rail width}/2$$

$$Ft_c = \frac{\text{inertia} \cdot m_{rail}}{2\pi \cdot \tan(\text{ear angle})} \tag{6.2}$$

The tension threshold here is around 16.6N, very close to the numerical results. In the real engines, this value may vary and even at very high engine speed when ID rail clearance opens and a significant amount of oil leak into groove, this only indicates there exists more oil behind the ring but not necessarily more oil consumption. We still need to build a bridge for oil to pass the upper rail.

6.5 Oil flow passing the upper flank groove clearance

After oil reaches TPOCR groove from lower rail flank clearance, upper rail groove flank clearance and rail liner interface are the two possible passages for oil to leak into the piston 3rd land. As discussed in chapter 4, open clearance, pressure difference and oil supply on the boundary are the three critical requisites for net oil transport. The inner end of upper flank is the groove, the pressure is roughly at atmosphere. The upper flank clearance OD is directly exposed to 3rd land, and most of the time 3rd land pressure is greater than atmosphere other than some compression stroke in low load working condition, so net gas flow is always positive from 3rd land to OCR groove except close throttle condition. Oil transport is more complicated due to the oil boundary conditions. For ID boundary, bulk oil from groove exists when inertia is pointing upwards around TDC area, while its timing is dependent on the oil saturation inside the groove. OD boundary oil is also driven by inertia force but it can come either from 3rd land or rail up scraping. From 2DLIF experiments, we do observe more oil accumulation in 3rd land at low load because the gas flow blows less oil and the groove clearance is mostly dry in expansion stroke. But it is also possible any oil reaches upper flank OD can be immediately flushed into the clearance. The exact oil boundary conditions for upper flank is not well understood. Considering these uncertainties, the oil boundary condition for upper flank in this section is based on pure inertia effect.

Figure 6-7 shows the accumulated oil through upper rail ID and OD and OD clearance throughout one engine cycle, for 700mBar/500mBar/300mBar intake pressure at 5000 rpm. Positive oil direction means the oil is releasing from upper flank OD to ID. The clearance data indicates the load impact in expansion and exhaust stroke, while intake/compression stroke rail behavior is similar. Starting from compression stroke, OD clearance opens and there exists oil at the boundary, then it is possible to flush the oil into upper groove clearance. This oil release is squeezed out later the OD clearance closes in the later compression stroke. The ID oil flow pattern also shows this releasing never reaches ID. In the expansion and exhaust stroke, due to the 3rd
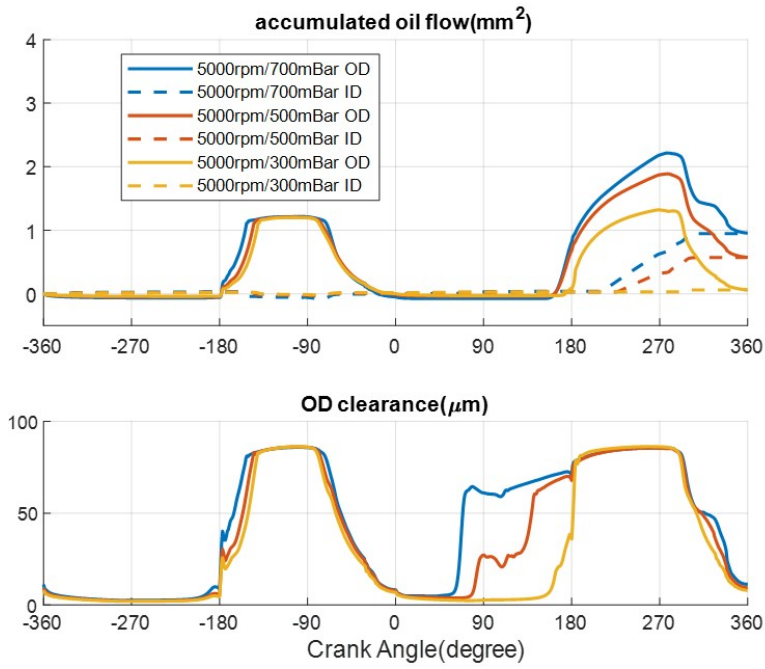
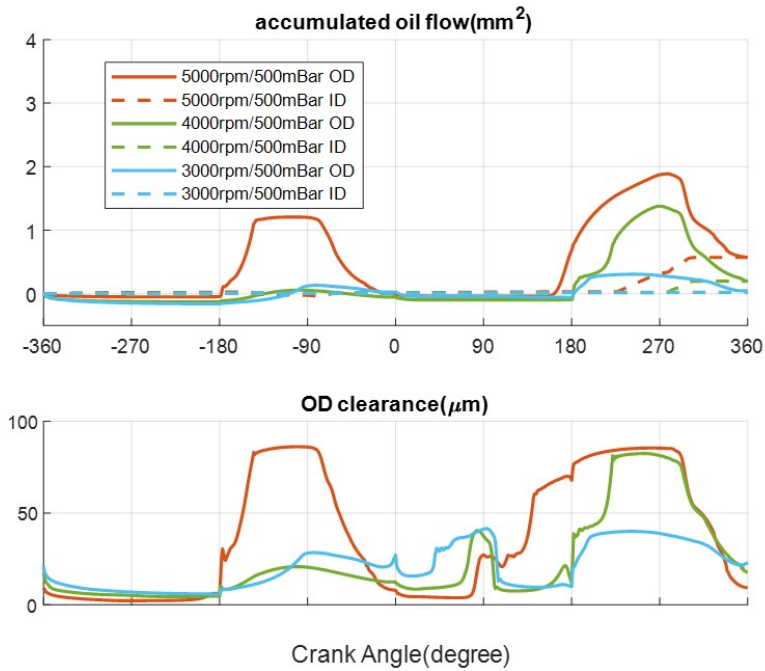Figure 6-7: Accumulated Oil Flow and Clearance through Upper Rail at 5000rpm

Figure 6-8: Accumulated Oil Flow and Clearance through Upper Rail at Different Speeds

land pressure the residence time of OD clearance opening lasts longer, so the third land oil is possible to reach ID as we can see net ID oil flow.

Figure 6-8 is the upper flank accumulated oil flow and clearance at different engine speed with same load. At 4000 and 3000 rpm, the OD clearance is not fully open in compression/exhaust stroke due to smaller inertia force, thus the oil release does not show the same peak at 5000 rpm case. In the exhaust stroke, with higher speed the clearance opens more and leads to greater oil flow. At further lower engine speed under 3000rpm, the inertia force is too small to lift the rail especially at ID, there is barely net oil transport in the groove.

From the modeling experience, although we didn't reach a highly confident boundary condition for the upper rail, it is difficult for upper rail to leak oil from groove to 3rd land. The most vulnerable moment is the compression stroke in low load conditions when 3rd land pressure is negative to atmosphere. The groove oil moves to the upper rail ID at the late compression stroke when inertia points upwards, meantime the rail clearance is also closed by inertia so oil passage is blocked. If the 3rd land pressure grows and reopens the clearance, at that time the pressure direction is already reversed so there wouldn't be oil leakage.

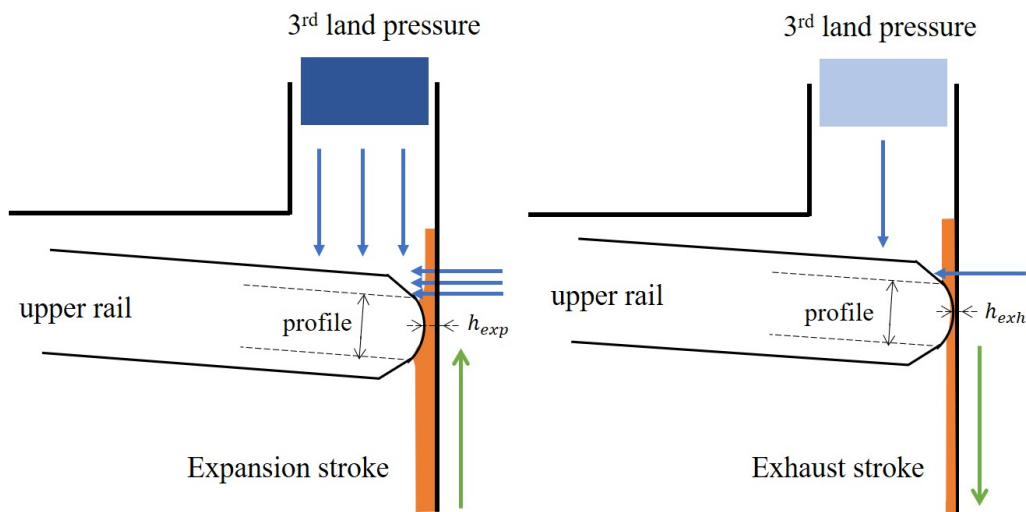## 6.6 Effects of load on liner oil up-scraping

Figure 6-9: 3rd Land Pressure Effect on Upper Rail Scraping

In chapter 4 we have discussed large 3rd land pressure will push upper rail in axial and radial direction so the rail will twist and move away from liner. The oil passing the rail liner interface highly depends on the exact clearance profile. The 3rd land pressure can reach up to a few bars due to combustion process in expansion stroke and usually drops to atmosphere level in exhaust stroke, this asymmetry of pressure difference allows more scraping ability in exhaust stroke than expansion stroke, so the trailing oil in expansion stroke tends to be up-scraped by exhaust stroke at higher engine loads, as shown in figure 6-9.

Figure 6-10 shows the predicted 3rd land pressure and rail liner minimum clearance for three different loads at 5000rpm and figure 6-11 is the trailing oil after rail pass. Figure 6-12 is the upper rail up-scraping rate. At higher load the 3rd land will see a higher pressure after combustion TDC. Rail liner clearance differs among different load especially in the expansion stroke. Notice the spike of clearance after TDC comes from our empirical inputs for oil supply timing at upper rail lower interface in down stroke, which is a relatively overestimation to illustrate the up-scraping effect. If the 3rd land pressure is very high, it is possible to push all the piece oil control ring to the lower flank as shown in figure 4-14 before expansion mid stroke, then lower rail
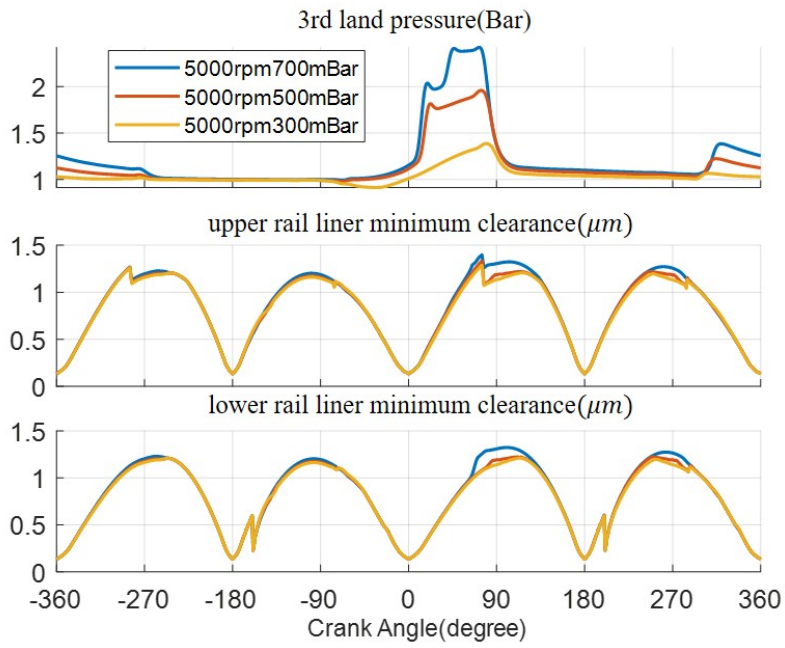
Figure 6-10: 3rd Land Pressure and Rail Liner Minimum Clearance with Different Loads at 5000rpm
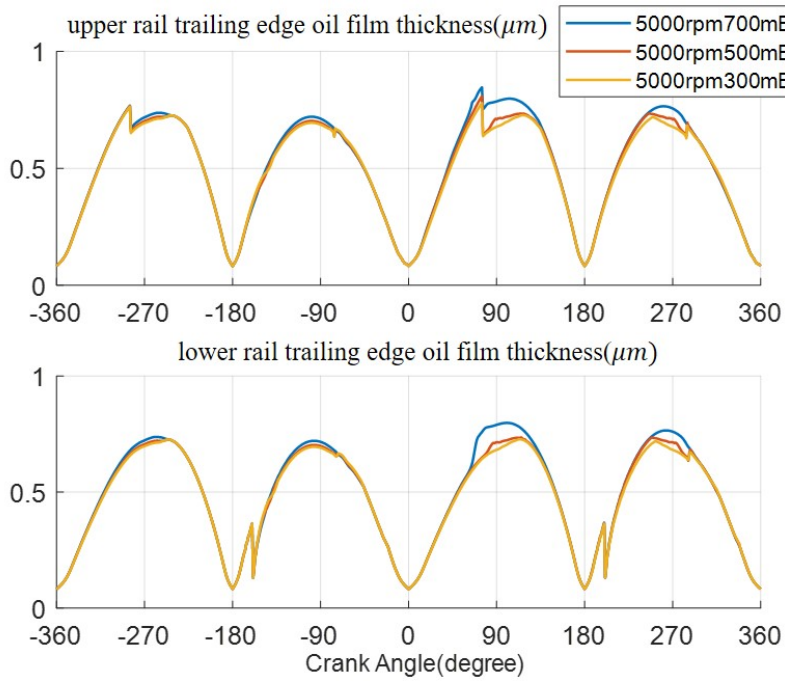

Figure 6-11: Liner Oil Film Thickness after Rail Pass with Different Loads at 5000rpm

returns neural twist instead of a positive twist favoring down stroke. This explains why 5000rpm/700mBar case lower rail allows more oil to pass even after 3rd land pressure drop. The left-over oil on the liner will feed into upper rail and most of it passes upper rail, considering upper rail sealing is more vulnerable compared with lower rail due to effective tension loss from 3rd land pressure. When 3rd land pressure drops and upper rail moves up in the exhaust stroke with higher interface pressure with liner, the oil will be up-scraped into the 3rd land and may potentially cause oil consumption.
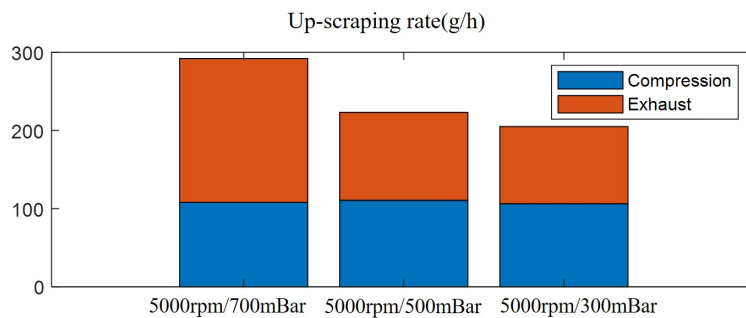
Figure 6-12: Up Scraping Rate at 5000rpm

From the rail dynamics perspective, higher load compromises the ring liner oil sealing. The additional 3rd land pressure will push both upper and lower rail towards negative twist in down stroke and create unbalanced effective tension between expansion and exhaust stroke in the radial direction. From 2DLIF experiments, it also suggests additional gas flow through the upper rail clearance may change the gas flow pattern in the expander pitches and force frequent bridging into upper rail, as shown in figure 6-13.

Figure 6-13: 2DLIF Gas Flow Comparison Intake Expansion

6.7 Effects of engine speed on up-scarping

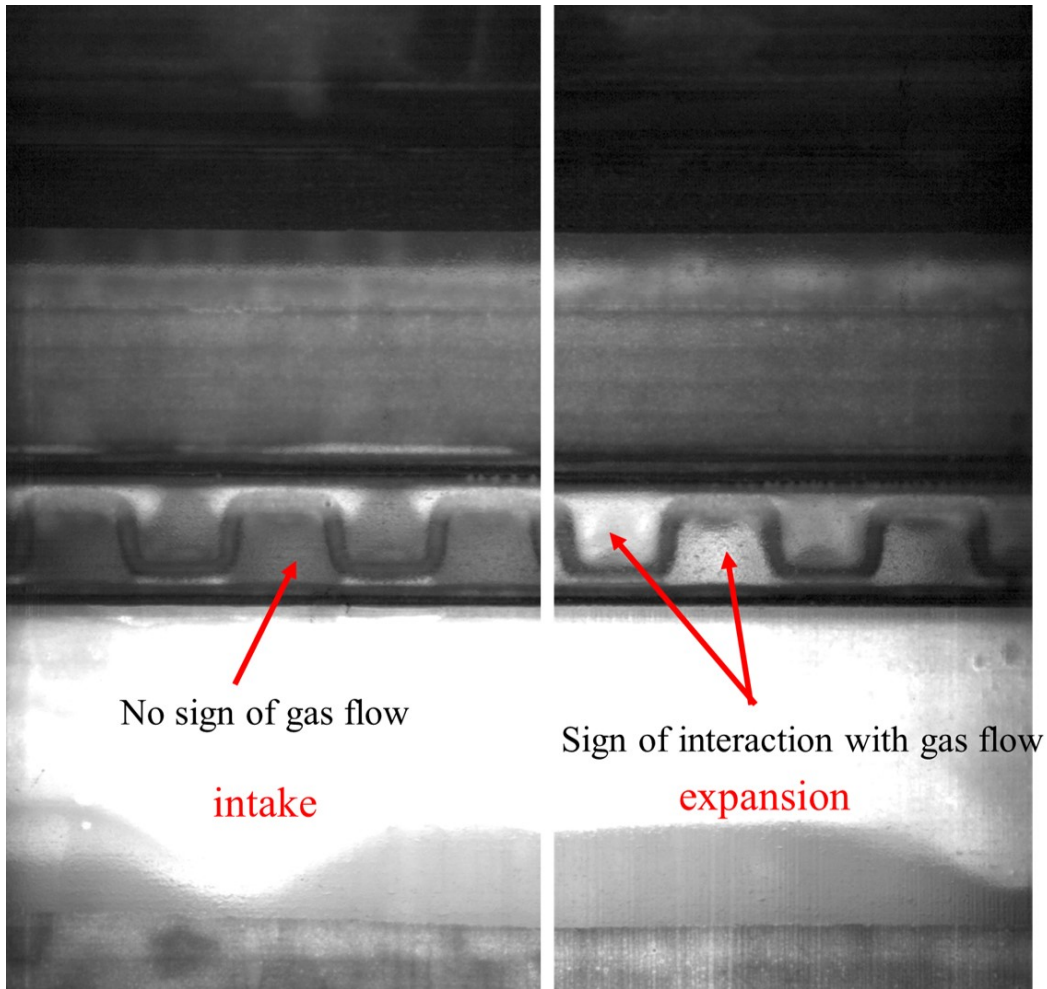In a well lubricated engine, rail liner lubrication is mostly hydrodynamics lubrication within engine stroke other than BDC and TDC area. The hydrodynamic lubrication pressure is proportional to $\mu U/h$, as shown in equation 2.25, where μ is the oil viscosity, U is the relative velocity between rail and liner, h is the clearance. The pressure should balance the rail tension, at higher engine speed, the rail liner will expect a larger clearance with greater liner velocity.

Figure 6-14 shows the trailing oil film thickness for upper rail and lower rail and figure 6-15 is the calculated up-scraping rate. The overall clearance and oil film thickness on the liner grows with the engine speed, allowing potential up-scraping

rate. Besides, engine operates more cycle at higher speed. Notice the calculated up-scraping rate here is mainly for trend analysis, since it is dependent on the bridging timing inputs which is same for all the cases in this section. According to Fang[6], bridging also favors high speed working conditions, it is safe to draw the conclusion high speed condition is more vulnerable to up scraping.
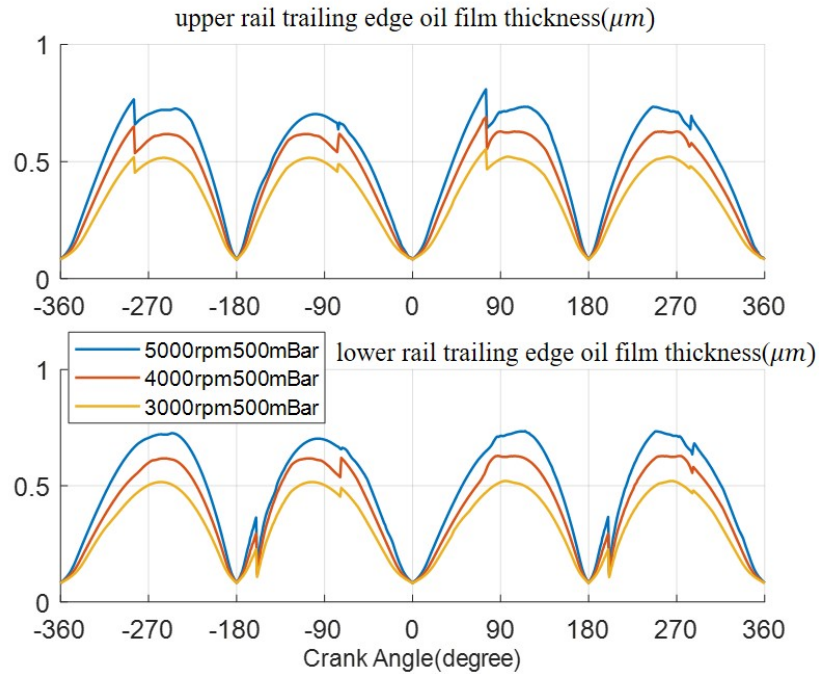

Figure 6-14: Liner Oil Film Thickness after Rail Pass at Different Speeds
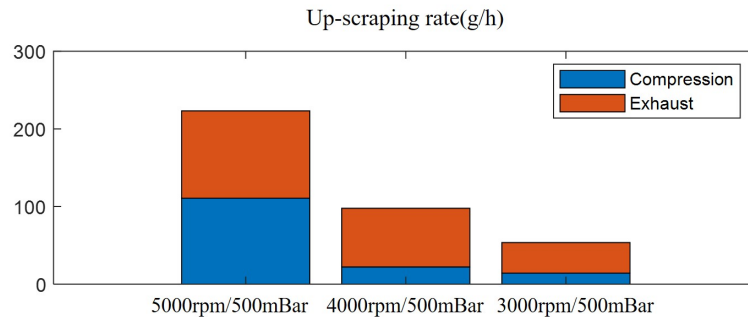
Figure 6-15: Up Scraping Rate at 500mBar

6.8 Summary and discussion on the oil transport around TPOCR

In this chapter, we systematically studied the oil leakages through upper/lower flank clearance and rail liner interface with different working conditions and design parameters. From previous industry experience, TPOCR usually performs well at low to intermediate working condition, after certain threshold, oil consumption grows rapidly with speed and load. Although the oil boundary conditions for the fluid models are not perfect and a system level mass conversation is not achieved, the result trend still gives us enough evidence to build a big picture of oil leakage mechanism around TPOCR, as shown in figure 6-16.

Figure 6-16: A Big Picture of Oil Flow around TPOCR

With the expander ear angle design and pumping suction force, the rail ID could seal the flank clearance at low speed. When engine is running at high engi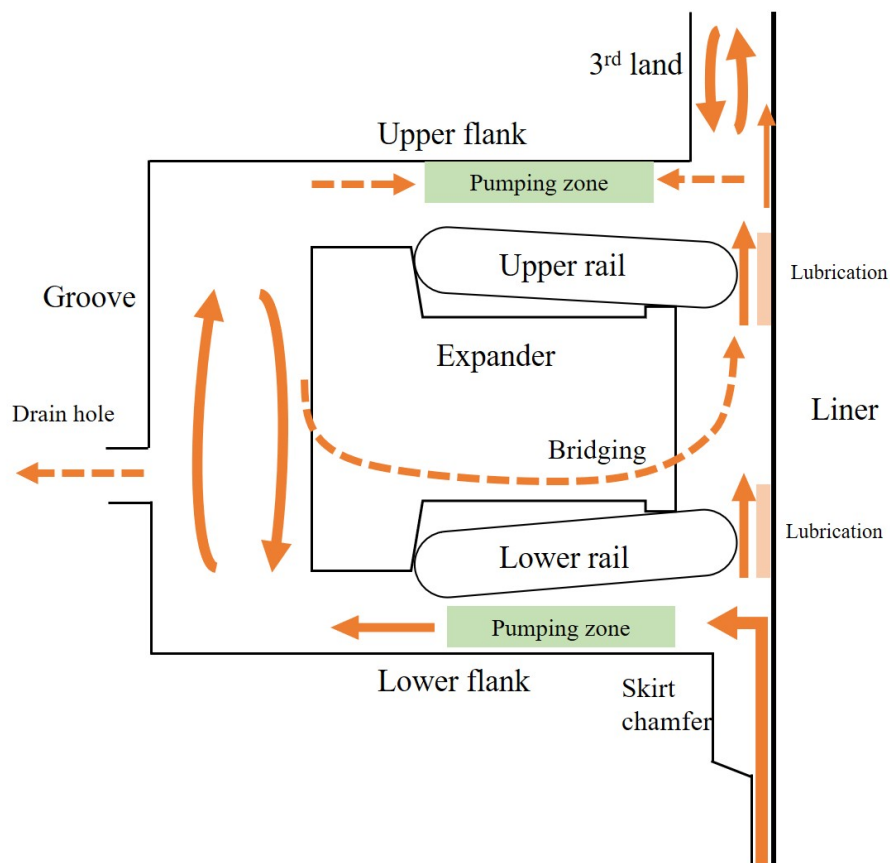ne speed, the inertia force drags the whole three pieces up and down so groove clearance can be open at certain crank angle. Besides, the higher relative velocity also creates clearance between liner and rail. For the oil movement, clearance is the necessary condition, this explains gasoline engines' low oil consumption at low engine speed.

Starting from skirt, higher engine speed induces dynamic pressure at lower clearance OD and lifts the lower rail so oil is allowed to get into the groove and build a dynamic mass balance. The major motion of groove oil is shaking up and down by inertia force. If oil is over filled, it is possible to release through the drop hole or reach the upper region. More importantly, as a combination of gas flow in the cross section, engine speed and groove oil accumulation, strong bridging effect is triggered to supply oil to upper rail liner interface.

From previous analysis, higher engine load resulting in higher 3rd land pressure leads to the strong gas flow and harass the sealing effect of upper rail. This can be the main reason for higher oil consumption at higher loads in gasoline engines.

The role of the upper flank clearance is to release the oil from the 3rd land, although we cannot eliminate the possibility of its leakage into the 3rd land especially in idle conditions. When 3rd land pressure is higher than groove, the net oil flow is towards groove. Besides, it is difficult to squeeze oil from ID to OD because this requires clearance, oil supply and pressure difference happening at the same time. In the experiments, we do see oil squeezed out into 3rd land from upper flank clearance, but given the simulation estimation, the source of this oil mainly comes from up-scraping or 3rd land.

Inside the 3rd land, there is another level of oil balance with inlet from up scraping and outlet through upper flank and towards upper region of piston. From the 2DLIF experiments, we observed 3rd land oil shaking up and down and more oil accumulation at low loads, this follows the intuition of 3rd land gas releasing. Besides, part of the up scraped oil stays on the liner and later directly contacts with 2nd ring, bypassing the control of 3rd land. This may be the next step on the oil consumption route after

TPOCR.

Above is the overview of oil transport mechanism around TPOCR, so far we've only studied the major patterns with in a 2D scenario. Circumferentially, depending on the relative location of TPOCR upper rail gap and drain holes, gas flow from 3rd land will push the oil towards the drain hole and helps releasing. Due to the structure of expander pitches, oil leveling occurs between neighbouring pitches. Besides the bulk oil motions due to inertia in the non-contact regions, surface tension effect also holds some oil at certain corners such as the upper flank clearance ID,OD boundary and generates additional pressure. Also the piston second motion can affect piston liner clearance and TPOCR behavior may differ along the circumferential direction. These are all possible directions for future work.

Chapter 7

Conclusion

7.1   Development and application of TPOCR model

In this work, a TPOCR model incorporating the ring dynamics and oil transport is developed to investigate the ring dynamics and oil regulation performance of TPOCR. The dynamic equations plays the role of main frame of the TPOCR model, coupling the sub-models describing the oil/gas transport and surrounding forces to the ring. Considering the fluid length scales, this model covers different fluid models for groove flank pumping, ring liner lubrication and groove oil movements. The groove pumping solves the pressure and oil distribution of a two phase Poiseuille flow with a convection equation. The rail liner lubrication is essentially the Reynolds Equation. These partial differential equations are implemented with numerical tricks to guarantee convergence.

For the groove oil movement, we proposed a method to speed up calculation with reduced order models, utilizing the non-linear property of neural network. Firstly an autoencoder is used to decompose the full space and later a recurrent neural network is used to learn the dynamic properties in the reduced space. The model generalizes the oil patterns in the groove and serves as the boundary condition for pumping model. This method is highly portable and can be adapted to other complex physical system modeling.

The TPOCR model is then applied to a typical gasoline engine and model results

are compared with the experimental images. In terms of rail motions, the simulation shows a good match with the experiments and explains the mechanisms behind the images. The experiment provides informative oil motions throughout the engine cycle, inspiring further improvement directions for oil models and boundary condition treatment.

The parametric study on the oil transport around TPOCR helps build a complete route of TPOCR oil leakage and explains the industry experience of gasoline engine oil consumption at high load high speed working conditions. The mechanism in different fluid passages are elaborated with various working conditions, other possible scenarios are discussed given the model assumption. Some TPOCR design parameters are studied to illustrate the reason behind industry optimization.

This comprehensive simulation package paves the way for understanding the TPOCR behavior and oil regulation mechanisms, it also facilitates the industry users to evaluate and refine the product performance. Communication and corporation from industry has been with the model development throughout the whole process, the model is robust and instructive with practical value.

7.2   Future work

Given the assumptions made in the model development and limitations of time, there are a few points worth notifying for future work.

Firstly, the model is based on axisymmetric assumptions. To study the circumferential effect, a full 3D structure is needed with the oil transport. Considering the periodic shape and small displacement of TPOCR expander, it is possible to represent the 3D structure with low order approximation to save the 3D computational time. For the flank clearance pumping model, more cross sections are needed for the circumferential effect and partial oil film scenario. Regarding the ring liner lubrication, a numerical solution may be needed to accommodate any general ring profile designs.

For the groove oil motions, there are many things to do around the model order reduction method with neural network. Practically, more CFD training data would

allow the groove oil model to interact with other sub-models with fully mass conservation around TPOCR. From the model order reduction perspective, it is worthwhile investigating the interpretability of autoencoder with physical explanation so physics prior can be included. The recurrent neural network representing reduced space dynamics may diverge when inputs deviates from training data, the stability of neural network needs to be improved.

Back to TPOCR itself, we have yet address the full physics picture, it requires time and thinking to explore more mechanisms from experiments or simulation.

Bibliography

[1] John B. Heywood. *Internal Combustion Engine Fundamentals*. McGraw-Hill, 1988.

[2] D. Richardson. Review of power cylinder friction for diesel engines. *Journal of Engineering for Gas Turbines and Power-transactions of The Asme - J ENG GAS TURB POWER-T ASME*, 122, 10 2000.

[3] Zhi Wang, Hui Liu, and Rolf Reitz. Knocking combustion in spark-ignition engines. *Progress in Energy and Combustion Science*, 61:78–112, 07 2017.

[4] Tian Tian. *Modeling the Performance of the Piston Ring-Pack in Internal Combustion Engines*. PhD thesis, Massachusetts Institute of Technology, Department of Mechanical Engineering, 1997.

[5] Tian Tian, Victor W. Wong, and John B. Heywood. Modeling the dynamics and lubrication of three piece oil control rings in internal combustion engines. In *SAE Technical Paper*. SAE International, 10 1998.

[6] Tianshi Fang. *Fluid Mechanics of Lubricant Transport in Non-Contact Regions in the Piston Ring Pack in Internal Combustion Engines*. PhD thesis, Massachusetts Institute of Technology, Department of Mechanical Engineering, 2019.

[7] Yuwei Li. unpublished Three-piece Oil Control Ring Structural Analysis. Talks at Lubrication in Internal Combustion Engines Consortium.

[8] Sebastian Ahling. unpublished 2DLIF experiments. Talks at Lubrication in Internal Combustion Engines Consortium.

[9] James Greenwood and J Tripp. The contact of two nominally flat rough surfaces. *Archive: Proceedings of The Institution of Mechanical Engineers 1847-1982 (vols 1-196)*, 185:625–634, 06 1970.

[10] Yuanzhong Hu, Herbert Cheng, Takayuki Arai, Kobayashiy, and Shunichi Aoyama. Numerical simulation of piston ring in mixed lubrication—a nonaxisymmetrical analysis. *Journal of Tribology*, 116:470–478, 07 1994.

[11] Yang Liu. *A Multi-scale Model Integrating both Global Ring Pack Behavior and Local Oil Transport in Internal Combustion Engines*. PhD thesis, Massachusetts Institute of Technology, Department of Mechanical Engineering, 2017.

[12] Peter Benner, Serkan Gugercin, and Karen Willcox. A survey of projection-based model reduction methods for parametric dynamical systems. *SIAM Review*, 57:483–531, 06 2015.

[13] Diederik P Kingma and Max Welling. Auto-encoding variational bayes, 2013.